Enhancing accuracy of finite-dimensional models for lithium-ion batteries, observer design and experimental validation

Mira Khalil, Romain Postoyan, Stéphane Raël

Enhancing Accuracy of Finite-Dimensional Models for Lithium-Ion Batteries, Observer Design and Experimental Validation

Mira Khalil[1,2], Romain Postoyan[1] and Stéphane Raël[2]

***Abstract*—Accurate estimation of the internal states of lithium-ion batteries is key towards improving their management for safety, efficiency and longevity purposes. Various approaches exist in the literature in this context, among which designing an observer based on an electrochemical model of the battery dynamics. With this approach, the performance of the observer depends on the accuracy of the considered model. It appears that electrochemical models, and thus their associated observers, typically require to be of high dimension to generate accurate internal variables. In this work, we present a method to mitigate this limitation by correcting the lithium concentrations generated by a general class of finite-dimensional electrochemical models such that they asymptotically match those generated by the original partial differential equations (PDE) they are based on, for constant input currents. These corrections apply to finite-dimensional models of any order of the considered class. The proposed corrections lead to a new state space model for which we design observers, whose global, robust convergences are supported by a Lyapunov analysis. Both numerical and experimental validations are presented, which show the improvement of the accuracy of the state estimates as a result of the proposed corrections.**

***Index Terms*—Lithium-ion batteries, electrochemical models, observers, Lyapunov stability.**

I. Introduction

With the increasing integration of applications that adopt lithium-ion batteries for their energy storage needs, ensuring their safe and efficient operation becomes of paramount importance. Proper monitoring of the battery state is thus needed, which can be achieved by the battery management system (BMS) provided it is fed with precise battery variables. Unfortunately, some key variables cannot be measured directly with sensors and they therefore need to be estimated. The state of charge (SOC), which is directly related to the lithium concentrations in the battery electrodes, is one example of an unmeasurable key battery variable that needs to be estimated.

The battery state estimation problem has been thoroughly investigated in the literature e.g., [1]–[4]. A common method is to design an observer based on a mathematical model of the battery internal dynamics e.g., [5]–[12]. Several types of battery models are available for this purpose, see e.g., [13]–[15]. In particular, electrochemical models are suitable to describe the battery internal dynamics. These models are expressed by a set of partial differential equations (PDE), which describe the following phenomena: lithium diffusion within electrode active materials, electron migration in electrodes, ion migration and diffusion within the electrolyte and electrochemical kinetics of lithium insertion/de-insertion at electrode/electrolyte interface. More details about electrochemical models can be found in e.g., [16], [17]. Although these models can accurately generate internal state variables, their mathematical structure is often too complex for observer design. For this reason, reduced electrochemical models are considered instead. One popular approach is assuming the particles within an electrode behave like an average particle, we talk of single particle models (SPM) as in e.g., [7], [8], [10], [18]–[21]. Giving that solving PDEs analytically or numerically can be computationally demanding and complex, the PDEs are usually turned into ordinary differential equations (ODE) via spatial discretization. A finite-dimensional model is thus obtained, which is convenient to design and implement an observer. Nevertheless, for the model to be faithful to the original PDEs, it typically needs to be of high dimension. This implies that the associated observer may also need to be of high dimension, which may make its design numerically challenging and may be an issue for its implementation.

In this work, we present a method to alleviate the need for finite-dimensional electrochemical models to be of high dimension to generate accurate variables. We consider for this purpose finite-dimensional SPMs, which include those in e.g., [7], [8], [10], [19], [20] as special cases. We then present a technique to systematically correct the concentrations generated by these models so that these asymptotically match the concentrations given by the original PDEs for constant currents. Hence, for any given model order, we obtain that the corrected concentrations from the finite-dimensional models asymptotically tend to the actual concentrations of the original infinite-dimensional model for constant inputs thereby asymptotically eliminating the errors induced by spatial discretization. Although the purpose of these corrections is to eliminate asymptotic errors for constant inputs, the provided simulation results show that significant improvements may also be obtained for short time horizons with a rapidly changing current profile. We then exploit these corrected concentrations to derive a new output voltage equation, which leads to a new state space model.

Afterwards, we present two methods to design an observer

*This work was supported by the French PIA project "Lorraine Université d'Excellence", reference ANR-15-IDEX-04-LUE.

[1]Université de Lorraine, CNRS, CRAN, F-54000 Nancy, France. (mira.khalil@univ-lorraine.fr, romain.postoyan@univ-lorraine.fr).

[2]Université de Lorraine, GREEN, F-54000 Nancy, France. (stephane.rael@univ-lorraine.fr).

for the new, corrected model. The first method consists in assuming that an observer has already been designed for the original model without correction, using for instance the results of e.g., [6], [7], [10], and we derive conditions under which the same observer structure still converges for the new model; we talk of observer emulation. If these conditions are not satisfied, an alternative is to directly design an observer for the new model. We present a method for this purpose, which is based on polytopic and Lyapunov-based tools similarly to e.g., [6], [11], [22]. This method guarantees the robust convergence of the state estimates generated by the observer to the actual battery states provided a linear matrix inequality holds. We then explain how to correct the estimated concentrations to asymptotically track those of the original PDEs in absence of disturbances and for constant inputs. Simulation results are presented to illustrate the improvements brought by the corrected model and the associated estimation schemes. An experimental validation of the obtained results is also provided, which shows that the cell voltage generated by the new, corrected model is improved by about 25% compared to the same model without correction, which results in an improved SOC estimate by about 25%.

Compared to the preliminary version of this work [23], completely novel elements include: (i) the generalization of the considered class of SPMs, which captures more general spatial discretizations; (ii) the detailed analysis of the concentrations correction; (iii) the emulation-based observer; (iv) the experimental validation of the results.

The rest of this paper is organised as follows. The considered class of SPMs is given in Section II. The correction of lithium concentrations is presented in Section III. The new state space model is derived in Section IV. The observers designs are presented in Section V. Numerical simulations are provided in Section VI. The obtained results are validated experimentally in Section VII. Section VIII concludes the paper. All the parameters used in the paper are summarized in Table I.

Notation. Let $\mathbb{R}$ be the set of real numbers, $\mathbb{R}_{>0} := (0,\infty)$, $\mathbb{R}_{\geq 0} := [0,\infty)$, $\mathbb{R}_{<0} := (-\infty,0)$, $\mathbb{Z}$ be the set of integers, $\mathbb{Z}_{>0} := \{1,2,3,...\}$ and $\mathbb{C}$ be the set of complex numbers. We use $\mathbb{I}_n$ to denote the identity matrix of dimension n, $\mathbf{0}_{n\times m}$ the zero matrix of $\mathbb{R}^{n\times m}$ and $\mathbf{1}_{n\times m}$ the matrix of $\mathbb{R}^{n\times m}$ whose elements are all equal to 1, with $n,m \in \mathbb{Z}_{>0}$. Given square matrices $A_1,...,A_n$, $\text{diag}(A_1,...,A_n)$ is the block diagonal matrix, whose block diagonal components are $A_1,...,A_n$ and $\underline{\text{diag}}(A_1,...,A_n)$ ($\overline{\text{diag}}(A_1,...,A_n)$) is the lower (upper) block diagonal matrix, whose lower (upper) block diagonal components are $A_1,...,A_n$. Given a real, symmetric matrix P, its maximum and minimum eigenvalues are denoted by $\lambda_{\max}(P)$ and $\lambda_{\min}(P)$ respectively. The symbol $*$ in a matrix stands for the symmetric term, i.e., $\left(\begin{smallmatrix} A & B \\ * & C \end{smallmatrix}\right) = \left(\begin{smallmatrix} A & B \\ B^\top & C \end{smallmatrix}\right)$. Given a vector $x \in \mathbb{R}^n$, $x^\top$ denotes the transpose of x. Given $x \in \mathbb{R}^n$ and $y \in \mathbb{R}^m$ with $n,m \in \mathbb{Z}_{>0}$, we use the notation (x,y) to denote $(x^\top, y^\top)^\top$. Given two functions $f,g : \mathbb{C} \to \mathbb{C}$, we write $f(x) \underset{x\to 0}{\sim} g(x)$ when $\lim_{x\to 0} \frac{f(x)}{g(x)} = 1$, in which case the functions f and g are said to be equivalent at 0. Given $f : \mathbb{R} \to \mathbb{R}^n$ with $n \in \mathbb{Z}_{>0}$, $(f)_\infty$ stands for $\lim_{t\to\infty} f(t)$ when it exists. For a vector $x \in \mathbb{R}^N$, $|x|$ denotes its Euclidean norm. For a matrix $A \in \mathbb{R}^{n\times m}$, $\|A\|$ stands for its 2-induced norm, $\ker(A) := \{x \in \mathbb{R}^m : Ax = \mathbf{0}_n\}$ and for any $i \in \mathbb{R}^n$, $j \in \mathbb{R}^m$, $(A)_{ij}$ represents the j-th element of the i-th row of matrix A. Let $f : \mathbb{R}_{\geq 0} \to \mathbb{R}^N$, $\|f\|_{\mathscr{L}_2,[0,t)}$ denotes the $\mathscr{L}_2$ norm of f on the interval $[0,t)$, where $t \in [0,\infty)$. We write $f \in \mathscr{L}_2$, when $\|f\|_{\mathscr{L}_2,[0,\infty)} < \infty$.

Table I
PARAMETER DEFINITION AND NUMERICAL VALUES

A_{cell}	Cell area [m^2]	0.8
F	Faraday constant [C.mol^{-1}]	96485
R	Gaz constant [$\text{J.K}^{-1}\text{.mol}^{-1}$]	8.3145
T	Temperature [K]	298.15
N_{pos} =N_{neg}	Number of samples of the positive and negative electrode	4
u_T	Thermal voltage ($u_T = \frac{RT}{F}$) [V]	
d_{pos}	Thickness of the positive electrode [μm]	36.4
d_{neg}	Thickness of the negative electrode [μm]	50
d_{sep}	Thickness of the separator [μm]	25.4
D_{pos}	Solid diffusion coefficient [$\text{m}^2\text{.s}^{-1}$]	3.7×10^{-16}
D_{neg}	Solid diffusion coefficient [$\text{m}^2\text{.s}^{-1}$]	2×10^{-16}
R_{pos}	Particle radius of positive electrode [μm]	1
R_{neg}	Particle radius of negative electrode [μm]	1
j_0^{pos}	Exchange current density of positive electrode [A.m^{-2}]	0.54
j_0^{neg}	Exchange current density of negative electrode [A.m^{-2}]	0.75
ε_{pos}	Active material volume fraction [-]	0.5
ε_{neg}	Active material volume fraction [-]	0.58
$\varepsilon_{e,\text{pos}}$	Electrolyte phase volume fraction [-]	0.33
$\varepsilon_{e,\text{neg}}$	Electrolyte phase volume fraction [-]	0.332
$\varepsilon_{e,\text{sep}}$	Electrolyte phase volume fraction [-]	0.5
σ_{pos}	Electronic conductivity [S/m]	10
σ_{neg}	Electronic conductivity [S/m]	100
κ_e	Ionic conductivity at 298.15 K [S/m]	0.63
Q_{cell}	Cell capacity [Ah]	6
Q	Lithium quantity in solid phase [Ah]	11.396
c_0^{pos}	Lithium concentration at $SOC = 0\%$ [mol.m^{-3}]	25699
c_0^{neg}	Lithium concentration at $SOC = 0\%$ [mol.m^{-3}]	2199
c_{100}^{pos}	Lithium concentration at $SOC = 100\%$ [mol.m^{-3}]	10324
c_{100}^{neg}	Lithium concentration at $SOC = 100\%$ [mol.m^{-3}]	11849
$c_{\text{max}}^{\text{pos}}$	Maximum concentration [mol.m^{-3}]	29461
$c_{\text{max}}^{\text{neg}}$	Maximum concentration [mol.m^{-3}]	17525

II. PRELIMINARIES ON THE CLASS OF SPMS

We present in this section the class of SPMs, whose lithium concentrations will then be corrected in Section III. We first briefly recall the main elements of a lithium-ion cell, namely: the positive electrode, the separator and the negative electrode, which are all immersed in the electrolyte, and two current collectors, see Figure 1 for an illustration. The electrolyte is an ionic solution that ensures ion transport within the battery. The porous separator is an electrical insulator that does not allow electrons to flow between the two electrodes. However, being porous, it allows the passage of ions via the electrolyte. The positive and negative electrodes consist of almost spherical particles of porous materials. The electrodes structure creates a surface of contact between the electrodes and the electrolyte producing electrochemical couples between them and thus introducing a potential difference between the positive and negative electrode. Further information about lithium-ion batteries can be found in e.g., [24].

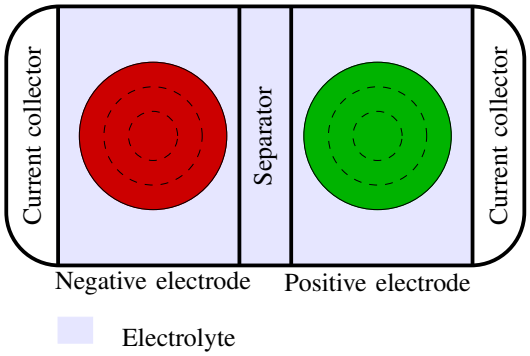

Figure 1. Battery model schematic.

We focus on models ensuring the next assumption.

Standing Assumption 1 (SA1): The following holds: (i) lithium insertion or de-insertion reactions are homogeneous along the thickness of each electrode; (ii) the electrolyte dynamics is neglected; (iii) the temperature of the cell is constant and homogeneous. □

Item (i) implies that each electrode can be reduced to a single particle, whose size is equal to the average size of all the particles that compose the actual electrode, we talk of SPM assumption, see e.g., [7], [8], [10], [19], [20]. As customarily done in electrochemical modeling of lithium-ion batteries, electrodes material particles are supposed spherical. In item (ii), we ignore the electrolyte dynamics, which is reasonable for moderate currents and moderate temperatures. For high current rates and/or low temperatures, item (ii) can be relaxed and electrolyte dynamics can be added to the presented model and observers by applying the results of [25] *mutatis mutandis*. In item (iii), we suppose that the temperature is constant however, when the temperature varies, and is measured we can adapt the model and the developed observers of Section V to take into account the temperature variation like in [6], [19]. As for the temperature homogeneity assumption, it is reasonable at moderate and high temperatures. For low temperatures, it may become invalid and be interpreted as a parametric uncertainty, which can be handled by the observers of Section V if the uncertainty is small enough, like in [19].

Given SA1, the main dynamical phenomenon is the lithium diffusion in the electrodes active particles. This phenomenon is described using the next PDEs (see e.g., [16]), for any $t \geq 0$ and $r \in [0, R_s]$, where $R_s > 0$ is the radius of the particle in electrode $s \in \{\text{neg}, \text{pos}\}$, with neg and pos denoting the negative and positive electrode, respectively,

$$\begin{array}{rcl} \varphi_s(r,t) & = & -D_s \frac{\partial c_s(r,t)}{\partial r} \\ \frac{\partial c_s(r,t)}{\partial t} & = & \frac{1}{r^2}\frac{\partial}{\partial r}\left(D_s r^2 \frac{\partial c_s(r,t)}{\partial r}\right), \end{array} \tag{1}$$

where c_s is the local concentration of lithium, φ_s is the lithium flux density and $D_s > 0$ is the diffusion coefficient of lithium, along the next couple of boundary conditions of Neumann type

$$\begin{array}{rcl} \varphi_s(0,t) & = & 0 \\ \varphi_s(R_s,t) & = & \frac{j_s^{\text{Li}}(t)}{a_s F}, \end{array} \tag{2}$$

where $j_s^{\text{Li}} \in \mathbb{R}$ is the electrochemical reaction rate, $a_s := \frac{3\varepsilon_s}{R_s}$ is the active surface per volume unit, $\varepsilon_s > 0$ is the volume fraction of the active material particle and $F > 0$ is Faraday's constant. The boundary condition at $r = 0$ means that there are no lithium flux in the center of the sphere. On the other hand, the boundary condition at $r = R_s$ means that the flux through the surface of the sphere is proportional to the electrochemical reaction rate. The mean lithium concentration of electrode s given by (1)-(2), denoted $c_{s,\text{mean}}$, is defined as, for all $t \geq 0$,

$$c_{s,\text{mean}}(t) := \frac{1}{V_s}\int_0^{R_s} 4\pi r^2 c_s(r,t)dr, \tag{3}$$

where $V_s := \frac{4}{3}\pi {R_s}^3$ is the volume of the particle of electrode s.

To derive a set of ODEs from (1)-(2), a spatial discretization method is performed. Hence, each particle is discretized into $N_s \in \mathbb{Z}_{>0}$ samples, where $s \in \{\text{neg}, \text{pos}\}$. A zero-order approximation is made, i.e., we assume that the lithium concentration in each sample, $c_{s,n}$ for $n \in \{1, ..., N_s\}$ and $s \in \{\text{neg}, \text{pos}\}$, is homogeneous. From the obtained set of ODEs, we derive the next state space equation, with the index $s \in \{\text{neg}, \text{pos}\}$

$$\dot{x}_s = A_s x_s + B_s m_s, \tag{4}$$

where $x_s := (c_{s,1}, \ldots, c_{s,N_s}) \in \mathbb{R}^{N_s}$ is the concatenation of the concentrations in electrode s and $m_s := -\frac{j_s^{\text{Li}}}{\varepsilon_s F} \in \mathbb{R}$ is the input. The matrices $A_s \in \mathbb{R}^{N_s \times N_s}$ and $B_s \in \mathbb{R}^{N_s \times 1}$ are defined as $A_s := \text{diag}(-\mu_1^s, -\upsilon_2^s, \ldots, -\upsilon_{N_s-1}^s, -\tilde{\mu}_{N_s}^s) + \overline{\text{diag}}(\tilde{\mu}_2^s, \ldots, \tilde{\mu}_{N_s}^s) + \overline{\text{diag}}(\mu_1^s, \ldots, \mu_{N_s-1}^s)$, $B_s := \begin{pmatrix} \mathbf{0}_{1\times(N_s-1)} & \frac{V_s}{V_{N_s}^s} \end{pmatrix}^\top$, where $\mu_i^s := \frac{S_i^s}{r_{i+1}^s - r_i^s}\frac{D_s}{V_i^s}$ for any $i \in \{1, \ldots, N_s - 1\}$, $\tilde{\mu}_i^s := \frac{S_{i-1}^s}{r_i^s - r_{i-1}^s}\frac{D_s}{V_i^s}$ for any $i \in \{2, \ldots, N_s\}$, $\upsilon_i^s := \tilde{\mu}_i^s + \mu_i^s$ for any $i \in \{2, \ldots, N_s - 1\}$, V_s is the particle volume, $V_i^s := \frac{4}{3}\pi((r_i^s)^3 - (r_{i-1}^s)^3)$ is the volume of sample i and $S_i^s := 4\pi(r_i^s)^2$ its external surface with $r_i^s > 0$ representing its external radius.

One of the lithium concentrations, namely $c_{\text{neg},1}$, is removed by exploiting the assumed lithium conservation, which is essential to design a converging observer. As a result, the dimension of the model is $N_{\text{neg}} + N_{\text{pos}} - 1$. We will return to this point in Section IV-B.

III. Concentrations correction

The spatial discretization of (1)-(2) to obtain (4) generates errors on the concentrations given by (4). These errors can be reduced by increasing the number of samples N_s, $s \in \{\text{neg}, \text{pos}\}$, but this leads to a high-dimensional system in (4), which may lead to computational issues, especially when using the model in (4) for observer design. We present in this section an alternative method to reduce these errors by correcting the lithium concentrations generated by (4) so that they asymptotically match those given by (1)-(2) for constant inputs for any number of spatial samples, as formalized in Section III-A. We can already emphasize that, although these corrections are established by considering the asymptotic behavior of the PDEs in (1) with the boundary conditions in (2) and the model in (4) for constant inputs, these may allow improving the accuracy of the concentrations given by (4) even for rapidly changing inputs as explained in Remark 2 and

illustrated in Sections VI and VII. In this section, we denote by $c_{s,(1)}$ the lithium concentrations generated from the PDEs in (1) with the boundary conditions in (2) and $c_{s,(4)} := x_s$ the lithium concentrations generated by model (4) for electrode s, with $s \in \{\text{neg}, \text{pos}\}$ for the sake of convenience.

A. Main result

We propose to correct the concentrations generated by model (4) as follows, for $j \in \{1, \dots, N_s\}$ and $s \in \{\text{neg}, \text{pos}\}$,

$$c_{s,\text{cor},j} := c_{s,(4),\text{mean}} - K_j^s (c_{s,(4),\text{mean}} - c_{s,(4),j}), \tag{5}$$

where $c_{s,\text{cor}}$ represents the corrected lithium concentrations of model (4), $c_{s,(4),\text{mean}} := \frac{1}{V_s} \sum_{n=1}^{N_s} V_n^s c_{s,(4),n}$ is the lithium-ion mean concentration in electrode s given by model (4) and $K_j^s \in \mathbb{R}$ is a static correction coefficient given by

$$K_j^s := \begin{cases} \dfrac{k(r_j^s)}{(\tilde{A}_s^{-1} \mathbf{1}_{(N_s-1)\times 1})_{j1}} & j \in \{1, \dots, N_s - 1\} \\ \dfrac{-k(r_j^s) V_{N_s}^s}{\Gamma_s^{\text{red}} \tilde{A}_s^{-1} \mathbf{1}_{(N_s-1)\times 1}} & j = N_s, \end{cases} \tag{6}$$

where $k(r_j^s) := \dfrac{\left(\frac{r_j^s}{R_s^s}\right)^2 - \frac{3}{5}}{6} \tau_s$, $\tau_s := \frac{R_s^2}{D_s}$, $\Gamma_s^{\text{red}} := \begin{pmatrix} V_1^s & V_2^s & \dots & V_{N_s-1}^s \end{pmatrix} \in \mathbb{R}^{1 \times N_s - 1}$, r_j^s is defined at the end of Section II and $\tilde{A}_s \in \mathbb{R}^{(N_s-1)\times(N_s-1)}$ is defined by $(\tilde{A}_s)_{ij} := (A_s)_{ij} - (A_s)_{iN_s} \frac{V_j^s}{V_{N_s}^s}$ for any $i, j \in \mathbb{R}^{N_s - 1}$.

We next present the main result of this section.

Theorem 1: For any constant input m_s, any corresponding solution $c_{s,(1)}$ to (1)-(2) and $c_{s,(4)}$ to (4) with $c_{s,(4),\text{mean}}(0) = c_{s,(1),\text{mean}}(0)$ satisfy for any $j \in \{1, \dots, N_s\}$ and $s \in \{\text{neg}, \text{pos}\}$

$$(c_{s,\text{cor},j} - c_{s,(1)}(r_j^s, \cdot))_\infty = 0, \tag{7}$$

where $c_{s,\text{cor}}$ is given in (5) and r_j^s is the external radius of each sample as defined after (4). □

Theorem 1 implies that, as time tends to infinity, the corrected concentrations defined in (5) match those generated by the PDEs in (1) with the boundary conditions in (2) when the input is constant. It is important to note that Theorem 1 imposes no conditions on the number of samples with which the PDEs in (1)-(2) are discretized, and thus no conditions on the dimension of (4) for (7) to hold.

To prove Theorem 1, we first analyze properties of the lithium concentrations of (1)-(2) in Section III-B and of the mean concentrations of (4) in Section III-C. We then investigate the error between the concentrations generated by the PDE model in (1)-(2) and model (4) in "steady state" in Section III-D. Lastly, we combine these properties to prove Theorem 1 in Section III-E.

Remark 1: The surface concentrations correction is illustrated in Figure 2, where the normalized step response of $c_{s,\text{mean}} - c_{s,\text{surf}}$, with $c_{s,\text{surf}}$ denoting the surface concentrations, is depicted for the PDE model in (1)-(2), taken as the reference model, and for model (4) with and without concentrations correction for different values of N_s. The error between the reference model and model (4) without correction is significant for $N_s = 5$. This error is reduced when increasing N_s to 50. On the other hand, this error is drastically reduced and eliminated in steady state for model (4) with correction by only taking $N_s = 5$ samples. Further numerical illustrations of the advantages of the proposed corrections are provided in Sections VI and VII. We note that this concentrations correction depends on the number of samples N_s, as the coefficient $K_{N_s}^s$ in (6) depends on N_s. In particular, the surface correction coefficient $K_{N_s}^s$ decreases as the number of samples N_s increases. This is consistent with what we see in Figure 2, where the error between the PDE model in (1)-(2) and the model in (4) without correction is reduced when increasing N_s. □

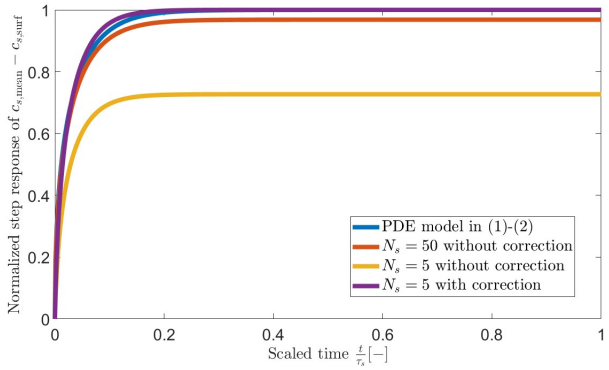

Figure 2. Normalized step response of $c_{s,\text{mean}} - c_{s,\text{surf}}$, with $s \in \{\text{neg}, \text{pos}\}$ and $c_{s,\text{surf}}$ represents the surface concentration of electrode s, for the PDE model in (1)-(2) and for model (4) with and without concentrations corrections.

Remark 2: The surface concentrations correction can only improve the accuracy of the model in (4) even for rapidly changing inputs. Indeed, it can be verified that $|Z_{\text{PDE model in (1)-(2)}}(t) - Z_{\text{model in (4) with correction}}(t)| \leq |Z_{\text{PDE model in (1)-(2)}}(t) - Z_{\text{model in (4) without correction}}(t)|$, where Z is the normalised step response of $c_{s,\text{mean}} - c_{s,\text{surf}}$ with $s \in \{\text{neg}, \text{pos}\}$ for all $t \geq 0$ and for $N_s \in \{2, \dots, 50\}$. We did not consider values of N_s bigger than 50 as in this case the model in (4) generates very accurate results with respect to the model in (1)-(2); recall that a motivation of our work is to make *low-dimensional* SPMs accurate. □

B. Properties of the concentrations for model (1)-(2)

The dynamics of the mean concentration of the PDEs in (1)-(2), i.e., $c_{s,(1),\text{mean}}$ given in (3), is obtained by integrating (1) over the particle volume and using the corresponding boundary conditions in (2), see Appendix A for more details. Thus, we derive that for any $t \geq 0$

$$\dot{c}_{s,(1),\text{mean}}(t) = m_s(t), \tag{8}$$

with $m_s(t) := -\frac{j_s^{\text{Li}}(t)}{\varepsilon_s F}$ as after (4).

We first have the next property, which states that any solution to (1)-(2) with an initial lithium concentrations profile $c_0(\cdot)$ converges to the solution to (1)-(2) initialized with a uniform lithium concentrations profile whose value is the mean of $c_0(\cdot)$ over $[0, R_s]$ with the same input m_s.

Proposition 1: Given any Lebesgue measurable, locally essentially bounded input m_s, consider $c_{s,(1),1}$ a solution to

(1)-(2) with $c_{s,(1),1}(r,0)=c_0(r)$ and $c_{s,(1),2}$ a solution to (1)-(2) with $c_{s,(1),2}(r,0)=\bar{c}_0$ for any $r\in[0,R_s]$, $\bar{c}_0\in\mathbb{R}_{\geq 0}$ being the initial mean concentration $c_{s,(1),1,\text{mean}}(0)$. For any $r\in[0,R_s]$,

$$(c_{s,(1),1}(r,\cdot)-c_{s,(1),2}(r,\cdot))_\infty=0. \tag{9}$$

□

The proof of Proposition 1 is postponed to Appendix B.

In view of Proposition 1, we focus on solutions to (1)-(2) with a uniform initial profile of lithium concentration in solid phase without loss of generality, i.e., there exists $\bar{c}_0\in\mathbb{R}_{\geq 0}$ such that for any $r\in[0,R_s]$ $c_{s,(1)}(r,0)=\bar{c}_0$, with $\bar{c}_0$ being the initial mean concentration $c_{s,(1),\text{mean}}(0)$. Let $c_{s,(1)}$ be a corresponding solution to (1)-(2), we derive in the Laplace domain (see [26]) that, for any $r\in[0,R_s]$ and $p\in\mathbb{C}$ the Laplace variable,

$$\begin{aligned}\mathscr{C}_s(r,p) &= F_s(r,p)m_s(p)\\ F_s(r,p) &:= \frac{\tau_s}{3}\frac{\sinh\left(r\sqrt{\frac{p}{D_s}}\right)\frac{R_s}{r}}{\sqrt{\tau_s p}\cosh(\sqrt{\tau_s p})-\sinh(\sqrt{\tau_s p})},\end{aligned} \tag{10}$$

where $\mathscr{C}_s(r,p)$ is the Laplace transform of $c_{s,(1)}(r,t)-c_{s,(1)}(r,0)$, $m_s(p)$ the Laplace transform of $m_s(t)$ and $\tau_s=\frac{R_s^2}{D_s}$ is the diffusion time constant. It follows from [26] that for any $r\in[0,R_s]$

$$F_s(r,p)\underset{p\to 0}{\sim}\frac{1}{p}+k(r), \tag{11}$$

where $k(r):=\frac{(\frac{r}{R_s})^2-\frac{3}{5}}{6}\tau_s$ is a constant as seen after (6).

In view of (10) and (11), we obtain, for a constant input m_s, $\mathscr{C}_s(r,p)\underset{p\to 0}{\sim}\frac{m_s(p)}{p}+k(r)m_s(p)$. On the other hand, the Laplace transform of (8) gives $\mathscr{C}_{s,\text{mean}}(p)=\frac{m_s(p)}{p}$, with $\mathscr{C}_{s,\text{mean}}$ the Laplace transform of $c_{s,(1),\text{mean}}(t)-c_{s,(1),\text{mean}}(0)$. Hence, $\mathscr{C}_s(r,p)\underset{p\to 0}{\sim}\mathscr{C}_{s,\text{mean}}(p)+k(r)m_s(p)$. In the time domain, for a constant input m_s and $c_{s,(1)}(r,0)=c_{s,(1),\text{mean}}(0)$, we derive that for any $r\in[0,R_s]$

$$(c_{s,(1)}(r,\cdot))_\infty=(c_{s,(1),\text{mean}})_\infty+k(r)m_s. \tag{12}$$

In view of (12), we deduce that, for any $r\in[0,R_s]$, the step response of the lithium concentrations of (1)-(2) tends to the mean concentration of model (1)-(2) up to an additional constant $k(r)m_s$. This property is exploited in Section III-D to evaluate the errors between the concentrations generated by model (1)-(2) and model (4). Before that, a property of the mean concentration for model (4) is established in the next section.

C. Properties of the mean concentration for model (4)

The mean lithium concentration in electrode s of model (4) is defined as

$$c_{s,(4),\text{mean}}:=\frac{1}{V_s}\sum_{n=1}^{N_s}V_n^s c_{s,(4),n}=\frac{1}{V_s}\Gamma_s x_s, \tag{13}$$

with $\Gamma_s:=\begin{pmatrix}V_1^s & V_2^s & \dots & V_{N_s}^s\end{pmatrix}\in\mathbb{R}^{1\times N_s}$. We have the next result on $c_{s,(4),\text{mean}}$.

Lemma 1: For any Lebesgue measurable, locally essentially bounded input m_s, any corresponding solution x_s to (4) satisfies $\dot{c}_{s,(4),\text{mean}}(t)=m_s(t)$ for all $t\geq 0$. □

Proof. Let m_s be a Lebesgue measurable, locally essentially bounded input and x_s be a corresponding solution to (4). In view of (4) and (13), we have $\dot{c}_{s,(4),\text{mean}}=\frac{1}{V_s}\Gamma_s\dot{x}_s=\frac{1}{V_s}\Gamma_s(A_s x_s+B_s m_s)$. On the other hand, matrix A_s in (4) satisfies $\Gamma_s A_s=\mathbf{0}_{1\times N_s}$. In addition, we have $\Gamma_s B_s=V_s$. Therefore, we obtain $\dot{c}_{s,(4),\text{mean}}(t)=m_s(t)$ for all $t\geq 0$. ■

Lemma 1 implies that the mean lithium concentration given by model (4) is equal to the mean concentration of the PDEs in (1)-(2) when these two are initialized at the same value i.e., when $c_{s,(1),\text{mean}}(0)=c_{s,(4),\text{mean}}(0)$, $c_{s,(1),\text{mean}}(t)=c_{s,(4),\text{mean}}(t)$ for any $t\geq 0$. The SPM in (4) is thus conservative with respect to mean concentrations, see [26]. We therefore use the short notation $c_{s,\text{mean}}$ in the following.

A consequence of this conservation property is that, by evaluating the normalized step response of $c_{s,\text{mean}}-c_s$ generated by model (1)-(2) and model (4), respectively, we obtain in steady state, provided it exists as we show next, a constant error. We present in the next section a method to determine this error, which we use to correct the concentrations as in (5).

D. Steady state errors

We define $\tilde{x}_s:=x_{s,\text{mean}}-x_s$ the mismatch between x_s and the vector of mean concentration $x_{s,\text{mean}}:=c_{s,\text{mean}}\mathbf{1}_{N_s\times 1}$. Using (4), Lemma 1 and the fact that $A_s\mathbf{1}_{N_s\times 1}=\mathbf{0}_{N_s\times 1}$, the dynamics of $\tilde{x}_s$ is given by

$$\dot{\tilde{x}}_s=A_s\tilde{x}_s+(\mathbf{1}_{N_s\times 1}-B_s)m_s. \tag{14}$$

The next lemma allows to write any element $\tilde{x}_{s,i}$ of any solution $\tilde{x}_s=(\tilde{x}_{s,1},\dots,\tilde{x}_{s,N_s})$ to (14) as a linear combination of all the others elements.

Lemma 2: For any Lebesgue measurable, locally essentially bounded input m_s, any corresponding solution $\tilde{x}_s$ to (14) satisfies $\sum_{i=1}^{N_s}V_i^s\tilde{x}_{s,i}(t)=0$ for all $t\geq 0$. □

Proof. Let m_s be a Lebesgue measurable, locally essentially bounded input and $\tilde{x}_s$ be a corresponding solution to (14). As $\tilde{x}_s=x_{s,\text{mean}}-x_s$, $\sum_{i=1}^{N_s}V_i^s\tilde{x}_{s,i}=\Gamma_s\tilde{x}_s=\Gamma_s c_{s,\text{mean}}\mathbf{1}_{N_s\times 1}-\Gamma_s x_s$. Given that $\Gamma_s\mathbf{1}_{N_s\times 1}=V_s$, $\sum_{i=1}^{N_s}V_i^s\tilde{x}_{s,i}(t)=V_s c_{s,\text{mean}}-\Gamma_s x_s$. In view of (13), $\sum_{i=1}^{N_s}V_i^s\tilde{x}_{s,i}=V_s\frac{1}{V_s}\Gamma_s x_s-\Gamma_s x_s$. Thus, we obtain $\sum_{i=1}^{N_s}V_i^s\tilde{x}_{s,i}(t)=0$ for all $t\geq 0$. ■

Using Lemma 2, we derive from (14),

$$\dot{\tilde{x}}_{s,\text{red}}=\tilde{A}_s\tilde{x}_{s,\text{red}}+\mathbf{1}_{(N_s-1)\times 1}m_s, \tag{15}$$

where $\tilde{x}_{s,\text{red}}$ represents the first N_s-1 components of $\tilde{x}_s$. Matrix $\tilde{A}_s\in\mathbb{R}^{N_s-1\times N_s-1}$ is defined as in Section III-A after (6) and satisfies the next result.

Lemma 3: $\tilde{A}_s$ is Hurwitz. □

The proof of Lemma 3 is provided in Appendix C to avoid breaking the flow of exposition.

Lemma 3 implies that, for a constant input m_s, any solution $\tilde{x}_{s,\text{red}}$ to (15) converges to a constant value, thereby proving the existence of steady states. For any given constant input m_s, the steady state of $\tilde{x}_{s,\text{red}}$ satisfies $(\dot{\tilde{x}}_{s,\text{red}})_\infty=(\tilde{A}_s\tilde{x}_{s,\text{red}}+\mathbf{1}_{(N_s-1)\times 1}m_s)_\infty=\mathbf{0}_{(N_s-1)\times 1}$. Therefore, we obtain

$$(\tilde{x}_{s,\text{red}})_\infty=-\tilde{A}_s^{-1}\mathbf{1}_{(N_s-1)\times 1}m_s, \tag{16}$$

noting that $\tilde{A}_s$ is invertible being Hurwitz by Lemma 3. In view of (16), $(c_{s,\text{mean}}-c_{s,(4),j})_\infty=-(\tilde{A}_s^{-1}\mathbf{1}_{(N_s-1)\times 1})_{j1}m_s$ for

any $j \in \{1,\dots,N_s-1\}$. On the other hand, we have from (12) that $(c_{s,\text{mean}} - c_{s,(1)}(r,\cdot))_\infty = -k(r)m_s$ for all $r \in [0,R_s]$. Hence, we obtain that for any $j \in \{1,\dots,N_s-1\}$

$$(c_{s,(4),j} - c_{s,(1)}(r_j^s,\cdot))_\infty = -k(r_j^s)m_s + (\tilde{A}_s^{-1}\mathbf{1}_{(N_s-1)\times 1})_{j1}m_s. \tag{17}$$

It remains to calculate the step response in steady state of $c_{s,(4),N_s} - c_{s,(1)}(r_{N_s}^s,\cdot)$. In view of Lemma 2, $\tilde{x}_{s,N_s} = -\frac{1}{V_{N_s}^s}\Gamma_s^{\text{red}}\tilde{x}_{s,\text{red}}$, Γ_s^{red} represent the N_s-1 first elements of Γ_s and defined after (6). Given (16), we derive

$$(\tilde{x}_{s,N_s})_\infty = \frac{1}{V_{N_s}^s}\Gamma_s^{\text{red}}\tilde{A}_s^{-1}\mathbf{1}_{(N_s-1)\times 1}m_s. \tag{18}$$

On the one hand, we have from (18) that $(c_{s,\text{mean}} - c_{s,(4),N_s})_\infty = \frac{1}{V_{N_s}^s}\Gamma_s^{\text{red}}\tilde{A}_s^{-1}\mathbf{1}_{(N_s-1)\times 1}m_s$. On the other hand, we have from (12) that $(c_{s,\text{mean}} - c_{s,(1)}(r,\cdot))_\infty = -k(r)m_s$ for all $r \in [0,R_s]$. Therefore, we obtain

$$\begin{aligned}(c_{s,(4),N_s} - c_{s,(1)}(r_{N_s}^s,\cdot))_\infty = &-k(r_{N_s}^s)m_s \\ &- \frac{1}{V_{N_s}^s}\Gamma_s^{\text{red}}\tilde{A}_s^{-1}\mathbf{1}_{(N_s-1)\times 1}m_s.\end{aligned} \tag{19}$$

To match the concentrations of model (4) to those of the PDEs in (1)-(2) in steady state, the corrected concentrations of model (4) need to satisfy $(c_{s,\text{cor},j} - c_{s,(1)}(r_j^s,\cdot))_\infty = 0$ for all $j \in \{1,\dots,N_s\}$. For this purpose, we introduce the correction coefficient K_j^s defined in (6) such as $(c_{s,\text{mean}} - c_{s,\text{cor},j})_\infty = K_j^s(c_{s,\text{mean}} - c_{s,(4),j})_\infty$. In the next section, we prove that the corrected concentrations match those of model (1)-(2) as stated in Theorem 1.

E. Proof of Theorem 1

We are now ready to prove Theorem 1. Let m_s be a constant input, $\bar{c}_0 \in \mathbb{R}_{\geq 0}$ and $c_{s,(1)}$ the solution to (1)-(2) with $c_{s,(1),\text{mean}}(0) = \bar{c}_0$. Let $c_{s,(4)}$ be the corresponding solution for model (4) with input m_s and initial condition $c_{s,(4),\text{mean}}(0) = \bar{c}_0$. In view of (5) and the property of the lithium concentrations of (1)-(2) presented in (12), we have, for any $j \in \{1,\dots,N_s\}$,

$$\begin{aligned}&(c_{s,\text{cor},j} - c_{s,(1)}(r_j^s,\cdot))_\infty \\ &\quad = \big(c_{s,(4),\text{mean}} - K_j^s(c_{s,(4),\text{mean}} - c_{s,(4),j}) - c_{s,(1),\text{mean}} \\ &\qquad\qquad -k(r_j^s)m_s\big)_\infty.\end{aligned} \tag{20}$$

Given the conservation property of the mean concentrations of model (4) with respect to model (1)-(2) established in Section III-C, (20) is equivalent to, for any $j \in \{1,\dots,N_s\}$,

$$\begin{aligned}&(c_{s,\text{cor},j} - c_{s,(1)}(r_j^s,\cdot))_\infty \\ &\qquad = (-K_j^s(c_{s,\text{mean}} - c_{s,(4),j}) - k(r_j^s)m_s)_\infty.\end{aligned} \tag{21}$$

Using the steady state error calculated in (16), we obtain for $j \in \{1,\dots,N_s-1\}$

$$\begin{aligned}&(c_{s,\text{cor},j} - c_{s,(1)}(r_j^s,\cdot))_\infty \\ &\qquad = K_j^s(\tilde{A}_s^{-1}\mathbf{1}_{(N_s-1)\times 1})_{j1}m_s - k(r_j^s)m_s.\end{aligned} \tag{22}$$

As for $j = N_s$, in view of (18), we derive

$$\begin{aligned}&(c_{s,\text{cor},j} - c_{s,(1)}(r_j^s,\cdot))_\infty \\ &\qquad = -K_j^s\frac{1}{V_{N_s}^s}\Gamma_s^{\text{red}}\tilde{A}_s^{-1}\mathbf{1}_{(N_s-1)\times 1}m_s - k(r_j^s)m_s.\end{aligned} \tag{23}$$

Given the expression of K_j^s in (6), we obtain from (22) and (23), for any $j \in \{1,\dots,N_s\}$, $(c_{s,\text{cor},j} - c_{s,(1)}(r_j^s,\cdot))_\infty = 0$ as in (7). This completes the proof.

IV. State space model

In this section, we exploit the results obtained in Section III to establish a new output equation for model (4), and thus a new state space model. Before that, the relation between m_s and the cell current I_{cell} is recalled. Then, a model reduction is performed as it is essential to ensure the system detectability, which is (implicitly) exploited later in Section V like in [5], [7], [10], [19].

A. Relation between m_s and I_{cell}

Given SA1, the electrochemical reaction rate is homogeneous within each electrode. Therefore, a proportional relationship can be established between I_{cell} and j_s^{Li} in particular $j_{\text{neg}}^{\text{Li}} := \frac{I_{\text{cell}}}{A_{\text{cell}}d_{\text{neg}}}$ and $j_{\text{pos}}^{\text{Li}} := -\frac{I_{\text{cell}}}{A_{\text{cell}}d_{\text{pos}}}$, where I_{cell} is in generator convention (i.e., $I_{\text{cell}} > 0$ in discharge), A_{cell} is the electrode surface and d_s is the thickness of electrode s. On the other hand, we have $m_s := -\frac{j_s^{\text{Li}}}{\varepsilon_s F}$. Hence, we obtain $m_{\text{neg}} := -\frac{I_{\text{cell}}}{\varepsilon_{\text{neg}}A_{\text{cell}}d_{\text{neg}}F}$ and $m_{\text{pos}} := \frac{I_{\text{cell}}}{\varepsilon_{\text{pos}}A_{\text{cell}}d_{\text{pos}}F}$.

B. Model reduction

Model (4) is reduced just like in e.g., [5], [7], [10], [19] by adopting the next assumption, which is essential later for the observer convergence.

Standing Assumption 2 (SA2): The quantity of lithium inserted in battery electrodes is constant and known. □

SA2 is reasonable over short periods of time. Factors such as cell degradation or side reactions can cause capacity loss over time, resulting in a reduction in the total quantity of lithium and the violation of SA2. In this case, if there is a small uncertainty regarding the quantity of lithium, the battery state and its estimation would exhibit asymptotic small errors, as shown by the Lyapunov-based proof in Theorems 2 and 3 in Section V. Conversely, if the uncertainty is big and thus the quantity of lithium needs to be estimated, state of health estimation algorithms may be employed as in e.g., [9], [27].

SA2 allows to write a lithium mass conservation. Hence, the quantity of lithium is defined as

$$Q := \alpha_{\text{neg}}\sum_{i=1}^{N_{\text{neg}}} c_{\text{neg},i}V_i^{\text{neg}} + \alpha_{\text{pos}}\sum_{i=1}^{N_{\text{pos}}} c_{\text{pos},i}V_i^{\text{pos}}, \tag{24}$$

where $\alpha_s := \frac{F}{3600}\frac{\varepsilon_s A_{\text{cell}}d_s}{V_s}$ and V_s is the volume of the particle of electrode s. From (24), we express the lithium concentration at the center of the negative electrode $c_{\text{neg},1}$ as a linear

combination of all the other sampled concentrations in solid phase

$$c_{\text{neg},1} = \overline{K} - \frac{1}{V_1^{\text{neg}}} \sum_{i=2}^{N_{\text{neg}}} c_{\text{neg},i} V_i^{\text{neg}} - \frac{\alpha_{\text{pos}}}{\alpha_{\text{neg}} V_1^{\text{neg}}} \sum_{i=1}^{N_{\text{pos}}} c_{\text{pos},i} V_i^{\text{pos}}, \tag{25}$$

where $\overline{K} := \frac{Q}{\alpha_{\text{neg}} V_1^{\text{neg}}}$.

In view of (25), $c_{\text{neg},1}$ is no longer needed in the state space representations as it can be recovered from the other concentrations.

C. Corrected output equation

We are ready to present the new output voltage equation. The output equation of model (4) is obtained by decomposition of the cell voltage V_{cell}. The main components of V_{cell} are the potential differences between the electrodes and the electrolyte called open circuit voltages (OCV) denoted OCV_s for $s \in \{\text{neg}, \text{pos}\}$, which depend on the surface insertion rates ζ_s defined by $\zeta_s := \frac{c_{s,N_s}}{c_{\max}^s}$ for $s \in \{\text{neg}, \text{pos}\}$, where $c_{\max}^s$ is the maximum lithium concentration of electrode s and c_{s,N_s} is the surface concentration generated by model (4). Given the correction of the lithium concentrations made in Section III, instead of using c_{s,N_s} to define the surface insertion rates, we use the corrected surface concentration c_{s,cor,N_s} defined in (5) to derive the corrected surface insertion rates $\zeta_{s,\text{cor}}$. As a result, we obtain the output equation for $y := V_{\text{cell}}$

$$y = OCV_{\text{pos}}(\zeta_{\text{pos,cor}}) - OCV_{\text{neg}}(\zeta_{\text{neg,cor}}) + g(u), \tag{26}$$

where $\zeta_{s,\text{cor}} := \frac{c_{s,\text{cor},N_s}}{c_{\max}^s}$ and $g(u) := -\eta_{r,\text{pos}}(u) - \eta_{\text{pos}}(u) - \eta_{\text{neg}}(u) - \eta_{r,\text{neg}}(u) - \eta_{r,\text{sep}}(u)$ for any $u := I_{\text{cell}} \in \mathbb{R}$, where $\eta_s(u) := 2\frac{RT}{F} \operatorname{asinh}\left(\frac{R_s}{6 j_0^s \varepsilon_s A_{\text{cell}} d_s} u\right)$, $\eta_{r,s}(u) := \frac{1}{2A_{\text{cell}}}\left(\frac{d_s}{\sigma_{s,\text{eff}}} + \frac{d_s}{\kappa_s}\right) u$, $\eta_{r,\text{sep}}(u) := \frac{1}{A_{\text{cell}}} \frac{d_{\text{sep}}}{\kappa_{\text{sep}}} u$, $\kappa_s := \kappa_e \varepsilon_{e,s}^{1.5}$, $\sigma_{s,\text{eff}} := \sigma_s \varepsilon_s$, $\kappa_{\text{sep}} := \kappa_e \varepsilon_{e,\text{sep}}^{1.5}$, with R, T, j_0^s, κ_e, $\varepsilon_{e,s}$, $\varepsilon_{e,\text{sep}}$, ε_s and σ_s defined in Table I.

Remark 3: The output equation in e.g., [7], [8], [10] is given by $y = OCV_{\text{pos}}(\zeta_{\text{pos}}) - OCV_{\text{neg}}(\zeta_{\text{neg}}) + g(u)$. The difference between this output equation and the one in (26) is in the determination of the OCVs. In (26), the OCVs are determined from the corrected surface concentrations as in the other output equation they are determined directly from the surface concentrations generated by (4). The term $g(u)$, on the other hand, remains the same for both output equations. □

D. State space form

We present the overall state space representation. We introduce for this purpose the state vector $x := (c_{\text{neg},2}, ..., c_{\text{neg},N_{\text{neg}}}, c_{\text{pos},1}, ..., c_{\text{pos},N_{\text{pos}}}) \in \mathbb{R}^N$ with $N := N_{\text{neg}} - 1 + N_{\text{pos}}$ (recall that $c_{\text{neg},1}$ has been removed in Section IV-B), the input $u = I_{\text{cell}} \in \mathbb{R}$, the output $y = V_{\text{cell}} \in \mathbb{R}$, and $w \in \mathbb{R}^{n_w}$ and $v \in \mathbb{R}^{n_v}$ represent additive exogenous perturbations and measurement noise respectively. We derive the next state space equation

$$\begin{cases} \dot{x} = Ax + Bu + K + Ew \\ y = h_{\text{cor}}(x) + g(u) + Dv, \end{cases} \tag{27}$$

where $A := \begin{pmatrix} A_1 & A_c \\ A_r & \operatorname{diag}(A_{\text{neg}}^{\text{red}}, A_{\text{pos}}) \end{pmatrix} \in \mathbb{R}^{N \times N}$, $A_1 := \left(-\upsilon_2^{\text{neg}} - \frac{V_2^{\text{neg}}}{V_1^{\text{neg}}} \mu_1^{\text{neg}}\right) \in \mathbb{R}^{1\times 1}$, $A_c := \left(\mu_2^{\text{neg}} - \frac{V_3^{\text{neg}}}{V_1^{\text{neg}}} \mu_1^{\text{neg}} \quad - \frac{V_{N_{\text{neg}}}^{\text{neg}}}{V_1^{\text{neg}}} \mu_1^{\text{neg}} \quad \dots \quad - \frac{\alpha_{\text{pos}} V_1^{\text{pos}}}{\alpha_{\text{neg}} V_1^{\text{neg}}} \mu_1^{\text{neg}} \quad \dots \quad - \frac{\alpha_{\text{pos}} V_{N_{\text{pos}}}^{\text{pos}}}{\alpha_{\text{neg}} V_1^{\text{neg}}} \mu_1^{\text{neg}}\right) \in \mathbb{R}^{1\times(N-1)}$, $A_r := \begin{pmatrix} \tilde{\mu}_3^{\text{neg}} & \mathbf{0}_{1\times(N-2)} \end{pmatrix}^\top \in \mathbb{R}^{(N-1)\times 1}$, $A_{\text{neg}}^{\text{red}} := \operatorname{diag}(-\upsilon_3^{\text{neg}}, \dots, -\upsilon_{N_{\text{neg}}-1}^{\text{neg}}, -\tilde{\mu}_{N_{\text{neg}}}^{\text{neg}}) + \underline{\operatorname{diag}}(\tilde{\mu}_4^{\text{neg}}, \dots, \tilde{\mu}_{N_{\text{neg}}}^{\text{neg}}) + \overline{\operatorname{diag}}(\mu_3^{\text{neg}}, \dots, \mu_{N_{\text{neg}}-1}^{\text{neg}}) \in \mathbb{R}^{(N_{\text{neg}}-2)\times(N_{\text{neg}}-2)}$, $B := \begin{pmatrix} \mathbf{0}_{1\times(N_{\text{neg}}-2)} & -\overline{K}_I^{\text{neg}} & \mathbf{0}_{1\times(N_{\text{pos}}-1)} & \overline{K}_I^{\text{pos}} \end{pmatrix}^\top \in \mathbb{R}^{N\times 1}$, $\overline{K}_I^s := \frac{V_s}{V_{N_s}^s \varepsilon_s F A_{\text{cell}} d_s}$ and $K := \begin{pmatrix} \mu_1^{\text{neg}} \overline{K} & \mathbf{0}_{1\times(N-1)} \end{pmatrix}^\top \in \mathbb{R}^{N\times 1}$. The matrices $E \in \mathbb{R}^{N\times n_w}$ and $D \in \mathbb{R}^{1\times n_v}$ allow to consider any type of noise and perturbations, and are therefore chosen in accordance with w and v. The function $h_{\text{cor}} : \mathbb{R}^N \to \mathbb{R}$ is defined as, for any $x \in \mathbb{R}^N$, $h_{\text{cor}}(x) := OCV_{\text{pos}}(H_{\text{pos,cor}} x) - OCV_{\text{neg}}(H_{\text{neg,cor}} x + K_1)$, such that $\zeta_{\text{pos,cor}} := H_{\text{pos,cor}} x$ and $\zeta_{\text{neg,cor}} := H_{\text{neg,cor}} x + K_1$, with $H_{s,\text{cor}} \in \mathbb{R}^{1\times N}$ defined as

$$\begin{aligned} H_{\text{pos,cor}} &:= \begin{pmatrix} \mathbf{0}_{1\times(N_{\text{neg}}-1)} & \overline{h}_1^{\text{pos}} & \dots & \overline{h}_{N_{\text{pos}}-1}^{\text{pos}} & \overline{h}_{N_{\text{pos}}}^{\text{pos}} + \frac{K_{N_{\text{pos}}}^{\text{pos}}}{c_{\max}^{\text{pos}}} \end{pmatrix} \\ H_{\text{neg,cor}} &:= \begin{pmatrix} \mathbf{0}_{1\times(N_{\text{neg}}-2)} & \frac{K_{N_{\text{neg}}}^{\text{neg}}}{c_{\max}^{\text{neg}}} & -h_1^* & \dots & -h_{N_{\text{pos}}}^* \end{pmatrix}, \end{aligned} \tag{28}$$

where $\overline{h}_i^s := \frac{V_i^s}{V_s c_{\max}^s}(1 - K_{N_s}^s)$, $h_i^* := \frac{V_i^{\text{pos}}}{V_{\text{neg}} c_{\max}^{\text{neg}}}(1 - K_{N_{\text{neg}}}^{\text{neg}}) \frac{\alpha_{\text{pos}}}{\alpha_{\text{neg}}}$ and the constant $K_1 := \overline{h}_1^{\text{neg}} \overline{K}$.

We are now ready to proceed with the observer design for system (27).

V. State estimation

In this section, we propose two methods to design a state observer for system (27), which both rely on an assumption made on the OCVs presented in Section V-A. The first one consists in assuming that an observer has been designed for the original model without correction and to derive conditions under which the same observer structure will be guaranteed to converge for the corrected model in (27), see Section V-B. If these conditions appear not to be satisfied, an alternative method is to directly design an observer for system (27). We propose a polytopic based approach for this purpose in Section V-C, similarly to e.g., [6], [11], [22]. We then explain how to correct the obtained state estimates, given by any of the two observers, to asymptotically match the concentrations given by the original PDEs in (1)-(2) for constant inputs by exploiting the results of Section III.

A. Assumption on the OCVs

We make the next assumption on the OCVs as in e.g., [6], [11], [19].

Assumption 1: For any $s \in \{\text{neg}, \text{pos}\}$, there exist constant matrices $C_{s,1}, C_{s,2} \in \mathbb{R}$ such as for any z, $z' \in \mathbb{R}$,

$$OCV_s(z) - OCV_s(z') = C_s(z, z')(z - z'), \tag{29}$$

where $C_s(z, z') := \lambda_1^s(z, z') C_{s,1} + \lambda_2^s(z, z') C_{s,2}$ with $\lambda_i^s(z, z') \in [0, 1]$ for $i \in \{1, 2\}$ and $\lambda_1^s(z, z') + \lambda_2^s(z, z') = 1$. □

Assumption 1 means that each OCV_s lies in a polytope defined by $C_{s,1}, C_{s,2}$ with $s \in \{\text{neg}, \text{pos}\}$. This condition is often verified in practice. Indeed, the OCVs are generally defined on the interval $[0,1]$ and are typically well-approximated by a piecewise continuously differentiable and thus globally Lipschitz function. Then, it suffices to extrapolate the OCVs on $[1,\infty)$ (resp. on $(-\infty,0]$) by using zero order or first order approximations based on the value of the OCVs at 1 (resp. at 0) for Assumption 1 to hold. Then, $C_{s,1}$ and $C_{s,2}$ represent the minimum and maximum slopes of OCV_s, respectively. This is the case for the OCVs considered in Sections VI and VII, see Figure 3.

B. Emulated observer

In this section, we derive conditions under which an observer designed for the original model without correction can still be applied for the corrected model (27). We first consider for this purpose the model without correction, given by

$$\begin{cases} \dot{x} = Ax + Bu + K + Ew \\ y = h(x) + g(u) + Dv, \end{cases} \tag{30}$$

where the function $h : \mathbb{R}^N \to \mathbb{R}$ is defined, for all $x \in \mathbb{R}^N$ by $h(x) := OCV_{\text{pos}}(H_{\text{pos}}x) - OCV_{\text{neg}}(H_{\text{neg}}x)$ as in Remark 3, with $H_{\text{pos}} := \begin{pmatrix} \mathbf{0}_{1\times N-1} & \frac{1}{c_{\max}^{\text{pos}}} \end{pmatrix}$ and $H_{\text{neg}} := \begin{pmatrix} \mathbf{0}_{1\times N_{\text{neg}}-2} & \frac{1}{c_{\max}^{\text{neg}}} & \mathbf{0}_{1\times N_{\text{pos}}} \end{pmatrix}$.

The designed observer is of the form

$$\begin{cases} \dot{\hat{x}} = A\hat{x} + Bu + K + L(y - \hat{y}) \\ \hat{y} = h(\hat{x}) + g(u), \end{cases} \tag{31}$$

where $\hat{x} \in \mathbb{R}^N$ is the state vector estimate, $L \in \mathbb{R}^N$ is the observation matrix gain and $\hat{y}$ is the estimated output. We assume that observer (31) is designed to satisfy the next Lyapunov properties.

Assumption 2: There exist P, $Q \in \mathbb{R}^{N\times N}$ symmetric, positive definite matrices and μ_w, $\mu_v \in \mathbb{R}_{>0}$ such that for any $x, \hat{x} \in \mathbb{R}^N$, $w \in \mathbb{R}^{n_w}$ and $v \in \mathbb{R}^{n_v}$, denoting $V(e_1) := e_1^\top P e_1$ and $e_1 := x - \hat{x}$,

$$\begin{aligned} &\langle \nabla V(e_1), Ae_1 + Ew - L(h(x) - h(\hat{x})) - LDv \rangle \\ &\qquad \le -e_1^\top Q e_1 + \mu_w |w|^2 + \mu_v |v|^2. \end{aligned} \tag{32}$$

□

Assumption 2 implies that system (30), (31) is $\mathscr{L}_2$-stable from (w,v) to $e_1 = x - \hat{x}$, in particular that there exist $c \ge 0$ and $\varepsilon \in \mathbb{R}_{>0}$ such that for any $w, v \in \mathscr{L}_2$ and any u Lebesgue measurable and locally essentially bounded, any solution $(x,\hat{x})$ to (30), (31) satisfies $\|e_1\|_{\mathscr{L}_2,[0,t)} \le c|e_1(0)| + \sqrt{\frac{\mu_w}{\varepsilon}}\|w\|_{\mathscr{L}_2,[0,t)} + \sqrt{\frac{\mu_v}{\varepsilon}}\|v\|_{\mathscr{L}_2,[0,t)}$ for any $t \ge 0$. Moreover, when $w = 0$ and $v = 0$, $\{(x,\hat{x}) : x = \hat{x}\}$ is uniformly globally exponentially stable, i.e., there exist $\gamma_1 \ge 1$, $\gamma_2 \in \mathbb{R}_{>0}$ such that for any u Lebesgue measurable and locally essentially bounded, any solution $(x,\hat{x})$ to (30), (31) satisfies $|e_1(t)| \le \gamma_1 |e_1(0)| e^{-\gamma_2 t}$ for any $t \ge 0$. Examples of observer designs ensuring the satisfaction of Assumption 2 for the non-corrected model (30) include, e.g., [6], [7], [10].

When feeding observer (31) with the new output equation (26), its convergence is no longer guaranteed in general. Our goal in this section is to identify sufficient conditions under which the same observer converges for model (27). We thus consider the next observer, which is observer (31) fed with the output equation (26)

$$\begin{cases} \dot{\hat{x}} = A\hat{x} + Bu + K + L(y - \hat{y}) \\ \hat{y} = h_{\text{cor}}(\hat{x}) + g(u), \end{cases} \tag{33}$$

Note that the difference with (31) is that $\hat{y}$ is defined using h_{cor} defined after (27) instead of h. We define the estimation error $e := x - \hat{x}$, whose dynamics follows from the difference of the dynamics of (27) and (33) as follows

$$\dot{e} = Ae + Ew - L(h_{\text{cor}}(x) - h_{\text{cor}}(\hat{x})) - LDv. \tag{34}$$

By adding and subtracting the term $L(h(x) - h(\hat{x}))$ to (34), we obtain

$$\dot{e} = Ae + Ew - L(h(x) - h(\hat{x})) - LDv + L(\tilde{h}(x) - \tilde{h}(\hat{x})), \tag{35}$$

where $\tilde{h} := h - h_{\text{cor}}$.

A consequence of Assumption 1 is that the term $\tilde{h}(x) - \tilde{h}(\hat{x})$ appearing in (35) can be written as, for any $x, x' \in \mathbb{R}^N$

$$\tilde{h}(x) - \tilde{h}(x') = \tilde{C}(x,x')(x - x'), \tag{36}$$

where $\tilde{C}(x,x') := \sum_{i=1}^4 \lambda_i(x,x')\tilde{C}_i$, with $\lambda_i(x,x') \in [0,1]$ for $i \in \{1,2,3,4\}$ and $\sum_{i=1}^4 \lambda_i(x,x') = 1$. This means that $\tilde{h}$ lies in a polytope defined by the vertices $\tilde{C}_i$ with $i \in \{1,2,3,4\}$, which are given in (43).

The next theorem presents the conditions under which observer (33) converges for system (27).

Theorem 2: Suppose the following holds.

(i) Assumptions 1 and 2 are satisfied.
(ii) Matrices P and Q in Assumption 2 satisfy

$$-Q + \tilde{C}_i^\top L^\top P + PL\tilde{C}_i < 0, \tag{37}$$

where $\tilde{C}_i$, with $i \in \{1,2,3,4\}$, defined in (43).

Then,

- system (27), (33) is $\mathscr{L}_2$-stable from (w,v) to e with gain less or equal to $\sqrt{\frac{\mu_w}{\varepsilon}}$ and $\sqrt{\frac{\mu_v}{\varepsilon}}$, respectively, where $\mu_w, \mu_v \in \mathbb{R}_{>0}$ come from Assumption 2 and $\varepsilon > 0$ is any constant satisfying $-Q + \tilde{C}_i^\top L^\top P + PL\tilde{C}_i \le -\varepsilon I_N$, in particular, there exists $c \ge 0$ such that for any $w, v \in \mathscr{L}_2$ and u Lebesgue measurable and locally essentially bounded input, any solution (x,e) to (27), (34) satisfies $\|e\|_{\mathscr{L}_2,[0,t)} \le c|e(0)| + \sqrt{\frac{\mu_w}{\varepsilon}}\|w\|_{\mathscr{L}_2,[0,t)} + \sqrt{\frac{\mu_v}{\varepsilon}}\|v\|_{\mathscr{L}_2,[0,t)}$ for any $t \ge 0$.
- $\{(x,e) : e = 0\}$ is uniformly globally exponentially stable when w=0 and v=0, i.e. there exist $\gamma_1 \ge 1$, $\gamma_2 \in \mathbb{R}_{>0}$ such that for any u Lebesgue measurable and locally essentially bounded input, any solution (x,e) to (27), (34) satisfies $|e(t)| \le \gamma_1 |e(0)| e^{-\gamma_2 t}$ for any $t \ge 0$. □

Proof. Let $x, \hat{x} \in \mathbb{R}^N$, $w \in \mathbb{R}^{n_w}$ and $v \in \mathbb{R}^{n_v}$. We consider $V(e) = e^\top P e$, where $e := x - \hat{x} \in \mathbb{R}^N$ as in Assumption 2. We have $\lambda_{\min}(P)|e|^2 \le V(e) \le \lambda_{\max}(P)|e|^2$ with $0 < \lambda_{\min}(P) \le$

$\lambda_{\max}(P)$ as P is symmetric, positive definite by Assumption 2. In view of (35),

$$\begin{aligned}\big\langle \nabla V(e), Ae+Ew-L(h(x)-h(\hat{x}))-LDv+L(\tilde{h}(x)-\tilde{h}(\hat{x}))\big\rangle \\ = 2(Ae+Ew-L(h(x)-h(\hat{x}))-LDv)^\top Pe \\ +2(L(\tilde{h}(x)-\tilde{h}(\hat{x})))^\top Pe, \quad (38)\end{aligned}$$

where we recall that $\tilde{h}=h-h_{\text{cor}}$. In view of Assumption 2,

$$\begin{aligned}2(Ae+Ew-L(h(x)-h(\hat{x}))-LDv)^\top Pe \\ \leq -e^\top Qe+\mu_w|w|^2+\mu_v|v|^2. \quad (39)\end{aligned}$$

By substituting the term $\tilde{h}(x)-\tilde{h}(\hat{x})$ in (38) by its expression in (36) and by using (39), we derive, omitting the argument of λ_i,

$$\begin{aligned}\langle \nabla V(e), Ae+Ew-L(h(x)-h(\hat{x}))-LDv+L(\tilde{h}(x)-\tilde{h}(\hat{x}))\rangle \\ \leq \sum_{i=1}^{4}\lambda_i\Big(-e^\top Qe+\mu_w|w|^2+\mu_v|v|^2+(L\tilde{C}_ie)^\top Pe \\ +e^\top PL\tilde{C}_ie\Big), \quad (40)\end{aligned}$$

recall that $\sum_{i=1}^4\lambda_i=1$. Given that matrices P and Q in Assumption 2 satisfy (37), there exist $\varepsilon\in\mathbb{R}_{>0}$ such that $-Q+\tilde{C}_i^\top L^\top P+PL\tilde{C}_i\leq-\varepsilon I_N$. We thus obtain

$$\begin{aligned}\langle \nabla V(e), Ae+Ew-L(h(x)-h(\hat{x}))-LDv+L(\tilde{h}(x)-\tilde{h}(\hat{x}))\rangle \\ \leq e^\top(-Q+\tilde{C}_i^\top L^\top P+PL\tilde{C}_i)e+\mu_w|w|^2+\mu_v|v|^2 \\ \leq -\varepsilon|e|^2+\mu_w|w|^2+\mu_v|v|^2. \quad (41)\end{aligned}$$

For any Lebesgue measurable and locally essentially bounded input current, the solutions to (27) are defined for all positive time as the right hand side of (27) is affine. We also have that for any Lebesgue measurable and locally essentially bounded input current u and output y, and any $w,v\in\mathscr{L}_2$, system (33) is forward complete as the only nonlinearity appearing in the right hand-side of (33) is due to h_{cor}, which is globally Lipschitz as a consequence of Assumption 1; see [28, Theorem 3.2]. In view of (41), for any $w,v\in\mathscr{L}_2$ and any solution x to (27) and $\hat{x}$ to (33), $e=x-\hat{x}$ verifies for all $t\geq0$

$$\dot{V}(e(t))\leq-\varepsilon|e(t)|^2+\mu_w|w(t)|^2+\mu_v|v(t)|^2,$$

which gives by [28, Lemma 3.4]

$$\begin{aligned}V(e(t))\leq V(e(0))-\varepsilon\int_0^t|e(\tau)|^2d\tau+\mu_w\int_0^t|w(\tau)|^2d\tau \\ +\mu_v\int_0^t|v(\tau)|^2d\tau.\end{aligned}$$

Consequently, as $V(e(t))\geq0$, $\sqrt{\int_0^t|e(\tau)|^2d\tau}\leq\sqrt{\frac{V(e(0))}{\varepsilon}+\frac{\mu_w}{\varepsilon}\int_0^t|w(\tau)|^2d\tau+\frac{\mu_v}{\varepsilon}\int_0^t|v(\tau)|^2d\tau}$ and thus $\|e\|_{\mathscr{L}_2,[0,t)}\leq\sqrt{\frac{V(e(0))}{\varepsilon}}+\sqrt{\frac{\mu_w}{\varepsilon}}\|w\|_{\mathscr{L}_2,[0,t)}+\sqrt{\frac{\mu_v}{\varepsilon}}\|v\|_{\mathscr{L}_2,[0,t)}$. Since $\lambda_{\min}(P)|e'|^2\leq V(e')\leq\lambda_{\max}(P)|e'|^2$, for any $e'\in\mathbb{R}^N$, we have $\sqrt{\frac{V(e(0))}{\varepsilon}}\leq\sqrt{\frac{\lambda_{\max}(P)}{\varepsilon}}|e(0)|$. With this, we obtain $\|e\|_{\mathscr{L}_2,[0,t)}\leq\sqrt{\frac{\lambda_{\max}(P)}{\varepsilon}}|e(0)|+\sqrt{\frac{\mu_w}{\varepsilon}}\|w\|_{\mathscr{L}_2,[0,t)}+\sqrt{\frac{\mu_v}{\varepsilon}}\|v\|_{\mathscr{L}_2,[0,t)}$, which implies the $\mathscr{L}_2$-stability of system (27), (33) as stated in Theorem 2.

For the case when $w=0$ and $v=0$, we have $\langle\nabla V(e),Ae+Ew-L(h(x)-h(\hat{x}))-LDv+L(\tilde{h}(x)-\tilde{h}(\hat{x}))\rangle\leq-\varepsilon|e|^2$ and $\lambda_{\min}(P)|e|^2\leq V(e)\leq\lambda_{\max}(P)|e|^2$. Therefore, we conclude the desired uniform global exponential stability property by following similar steps as in the proof of [28, Theorem 4.10]. ■

In addition to Assumptions 1 and 2, Theorem 2 also requires (37) to hold, which is a robustness property of observer (31) with respect to $h_{\text{cor}}-h$. This condition is needed to ensure that the observer still provides satisfactory convergence properties when using h_{cor} instead of h to generate the estimated output, as in (33). A solution is not always guaranteed to exist for (37): it depends on the model parameters and on the OCV curves. However, condition (37) can be easily tested numerically for given parameters and OCVs maximum and minimum slopes.

C. Polytopic approach

In this section, we directly synthesize an observer for system (27) by following a similar approach as in [6], [11], [22]. The proposed observer takes the same form as in (33). However, in this section, L is to be designed and not given by Assumption 2. We consider the estimation error $e:=x-\hat{x}$, whose dynamics is the same as in (34).

Another consequence of Assumption 1 is that the term $h_{\text{cor}}(x)-h_{\text{cor}}(x')$ appearing in (34) can be written as, for any $x,x'\in\mathbb{R}^N$

$$h_{\text{cor}}(x)-h_{\text{cor}}(x')=C(x,x')(x-x'), \quad (42)$$

where $C(x,x'):=\sum_{i=1}^4\Lambda_i(x,x')C_i$, with $C_i\in\mathbb{R}^N$ defined in (44), $\Lambda_i(x,x')\in[0,1]$ for $i\in\{1,2,3,4\}$ and $\sum_{i=1}^4\Lambda_i(x,x')=1$. This means that h_{cor} lies in a polytope defined by the vertices C_i with $i\in\{1,2,3,4\}$ in (44). Note the calculation of those vertices differ from those in (43) because of the change in the arguments of the OCVs in the output equation of the new model, see Section IV-C.

In view of (42), the estimation error dynamics can be written as

$$\dot{e}=(A-LC(x,\hat{x}))e+Ew-LDv. \quad (45)$$

The next theorem provides a sufficient condition to design gain $L\in\mathbb{R}^N$ under which $e=0$ is globally exponentially stable in absence of noise v and disturbance w, and satisfies $\mathscr{L}_2$-stability properties when the latter are non-zero.

Theorem 3: Suppose Assumption 1 holds and there exist $\varepsilon,\mu_w,\mu_v\in\mathbb{R}_{>0}$, $L\in\mathbb{R}^N$ and $P\in\mathbb{R}^{N\times N}$ symmetric and positive definite such that for any $i\in\{1,...,4\}$

$$\begin{pmatrix}\mathscr{H}_i+\varepsilon I_N & PE & -PLD\\ * & -\mu_wI_{n_w} & 0\\ * & * & -\mu_vI_{n_v}\end{pmatrix}\leq0, \quad (46)$$

with $\mathscr{H}_i:=(A-LC_i)^TP+P(A-LC_i)$ then system (27), (33) is $\mathscr{L}_2$-stable from (w,v) to e with gain less or equal to $\sqrt{\frac{\mu_w}{\varepsilon}}$ and $\sqrt{\frac{\mu_v}{\varepsilon}}$, respectively, and $e=0$ uniformly globally exponentially stable when w=0 and v=0. □

$$\begin{aligned}
\tilde{C}_1 &:= \begin{pmatrix} \mathbf{0}_{1\times(N_{\text{neg}}-2)} & \left(-\frac{1}{c^{\text{neg}}_{\max}}+\frac{K^{\text{neg}}_{N_{\text{neg}}}}{c^{\text{neg}}_{\max}}\right)C_{\text{neg},1} & -\overline{h}^{\text{pos}}_1 C_{\text{pos},1}-h^*_1 C_{\text{neg},1} & \dots & -\overline{h}^{\text{pos}}_{N_{\text{pos}}-1}C_{\text{pos},1}-h^*_{N_{\text{pos}}-1}C_{\text{neg},1} & \left(\frac{1}{c^{\text{pos}}_{\max}}-\overline{h}^{\text{pos}}_{N_{\text{pos}}}-\frac{K^{\text{pos}}_{N_{\text{pos}}}}{c^{\text{pos}}_{\max}}\right)C_{\text{pos},1}-h^*_{N_{\text{pos}}}C_{\text{neg},1} \end{pmatrix} \\
\tilde{C}_2 &:= \begin{pmatrix} \mathbf{0}_{1\times(N_{\text{neg}}-2)} & \left(-\frac{1}{c^{\text{neg}}_{\max}}+\frac{K^{\text{neg}}_{N_{\text{neg}}}}{c^{\text{neg}}_{\max}}\right)C_{\text{neg},1} & -\overline{h}^{\text{pos}}_1 C_{\text{pos},2}-h^*_1 C_{\text{neg},1} & \dots & -\overline{h}^{\text{pos}}_{N_{\text{pos}}-1}C_{\text{pos},2}-h^*_{N_{\text{pos}}-1}C_{\text{neg},1} & \left(\frac{1}{c^{\text{pos}}_{\max}}-\overline{h}^{\text{pos}}_{N_{\text{pos}}}-\frac{K^{\text{pos}}_{N_{\text{pos}}}}{c^{\text{pos}}_{\max}}\right)C_{\text{pos},2}-h^*_{N_{\text{pos}}}C_{\text{neg},1} \end{pmatrix} \\
\tilde{C}_3 &:= \begin{pmatrix} \mathbf{0}_{1\times(N_{\text{neg}}-2)} & \left(-\frac{1}{c^{\text{neg}}_{\max}}+\frac{K^{\text{neg}}_{N_{\text{neg}}}}{c^{\text{neg}}_{\max}}\right)C_{\text{neg},2} & -\overline{h}^{\text{pos}}_1 C_{\text{pos},1}-h^*_1 C_{\text{neg},2} & \dots & -\overline{h}^{\text{pos}}_{N_{\text{pos}}-1}C_{\text{pos},1}-h^*_{N_{\text{pos}}-1}C_{\text{neg},2} & \left(\frac{1}{c^{\text{pos}}_{\max}}-\overline{h}^{\text{pos}}_{N_{\text{pos}}}-\frac{K^{\text{pos}}_{N_{\text{pos}}}}{c^{\text{pos}}_{\max}}\right)C_{\text{pos},1}-h^*_{N_{\text{pos}}}C_{\text{neg},2} \end{pmatrix} \\
\tilde{C}_4 &:= \begin{pmatrix} \mathbf{0}_{1\times(N_{\text{neg}}-2)} & \left(-\frac{1}{c^{\text{neg}}_{\max}}+\frac{K^{\text{neg}}_{N_{\text{neg}}}}{c^{\text{neg}}_{\max}}\right)C_{\text{neg},2} & -\overline{h}^{\text{pos}}_1 C_{\text{pos},2}-h^*_1 C_{\text{neg},2} & \dots & -\overline{h}^{\text{pos}}_{N_{\text{pos}}-1}C_{\text{pos},2}-h^*_{N_{\text{pos}}-1}C_{\text{neg},2} & \left(\frac{1}{c^{\text{pos}}_{\max}}-\overline{h}^{\text{pos}}_{N_{\text{pos}}}-\frac{K^{\text{pos}}_{N_{\text{pos}}}}{c^{\text{pos}}_{\max}}\right)C_{\text{pos},2}-h^*_{N_{\text{pos}}}C_{\text{neg},2} \end{pmatrix}.
\end{aligned} \tag{43}$$

$$\begin{aligned}
C_1 &:= \begin{pmatrix} \mathbf{0}_{1\times(N_{\text{neg}}-2)} & -\frac{K^{\text{neg}}_{N_{\text{neg}}}}{c^{\text{neg}}_{\max}}C_{\text{neg},1} & \overline{h}^{\text{pos}}_1 C_{\text{pos},1}+h^*_1 C_{\text{neg},1} & \dots & \overline{h}^{\text{pos}}_{N_{\text{pos}}-1}C_{\text{pos},1}+h^*_{N_{\text{pos}}-1}C_{\text{neg},1} & \left(\overline{h}^{\text{pos}}_{N_{\text{pos}}}+\frac{K^{\text{pos}}_{N_{\text{pos}}}}{c^{\text{pos}}_{\max}}\right)C_{\text{pos},1}+h^*_{N_{\text{pos}}}C_{\text{neg},1} \end{pmatrix} \\
C_2 &:= \begin{pmatrix} \mathbf{0}_{1\times(N_{\text{neg}}-2)} & -\frac{K^{\text{neg}}_{N_{\text{neg}}}}{c^{\text{neg}}_{\max}}C_{\text{neg},1} & \overline{h}^{\text{pos}}_1 C_{\text{pos},2}+h^*_1 C_{\text{neg},1} & \dots & \overline{h}^{\text{pos}}_{N_{\text{pos}}-1}C_{\text{pos},2}+h^*_{N_{\text{pos}}-1}C_{\text{neg},1} & \left(\overline{h}^{\text{pos}}_{N_{\text{pos}}}+\frac{K^{\text{pos}}_{N_{\text{pos}}}}{c^{\text{pos}}_{\max}}\right)C_{\text{pos},2}+h^*_{N_{\text{pos}}}C_{\text{neg},1} \end{pmatrix} \\
C_3 &:= \begin{pmatrix} \mathbf{0}_{1\times(N_{\text{neg}}-2)} & -\frac{K^{\text{neg}}_{N_{\text{neg}}}}{c^{\text{neg}}_{\max}}C_{\text{neg},2} & \overline{h}^{\text{pos}}_1 C_{\text{pos},1}+h^*_1 C_{\text{neg},2} & \dots & \overline{h}^{\text{pos}}_{N_{\text{pos}}-1}C_{\text{pos},1}+h^*_{N_{\text{pos}}-1}C_{\text{neg},2} & \left(\overline{h}^{\text{pos}}_{N_{\text{pos}}}+\frac{K^{\text{pos}}_{N_{\text{pos}}}}{c^{\text{pos}}_{\max}}\right)C_{\text{pos},1}+h^*_{N_{\text{pos}}}C_{\text{neg},2} \end{pmatrix} \\
C_4 &:= \begin{pmatrix} \mathbf{0}_{1\times(N_{\text{neg}}-2)} & -\frac{K^{\text{neg}}_{N_{\text{neg}}}}{c^{\text{neg}}_{\max}}C_{\text{neg},2} & \overline{h}^{\text{pos}}_1 C_{\text{pos},2}+h^*_1 C_{\text{neg},2} & \dots & \overline{h}^{\text{pos}}_{N_{\text{pos}}-1}C_{\text{pos},2}+h^*_{N_{\text{pos}}-1}C_{\text{neg},2} & \left(\overline{h}^{\text{pos}}_{N_{\text{pos}}}+\frac{K^{\text{pos}}_{N_{\text{pos}}}}{c^{\text{pos}}_{\max}}\right)C_{\text{pos},2}+h^*_{N_{\text{pos}}}C_{\text{neg},2} \end{pmatrix}.
\end{aligned} \tag{44}$$

The proof of Theorem 3 follows the same steps as in [6, Theorem 1] and is therefore omitted. Theorem 3 means that we can design L to ensure the exponential convergence of the state estimate to the true state whenever (46) is verified. The matrix inequality in (46) is not linear, however it becomes linear after a standard change of variables, namely $W = PL$. Condition (46) can be easily tested given the model parameters and OCVs maximum and minimum slopes as done in Section VI-B. Also, the order reduction performed in Section IV-B appears to be essential for its feasibility, see also [19] where a similar condition is imposed for a different battery model.

Remark 4: Although Kalman filters are known for their ability to handle modeling uncertainties effectively, nonlinear Kalman filters generally lack global analytical convergence guarantees, contrary to the observer we propose in Section V-C. In addition, the implementation of nonlinear Kalman filters requires at least $N+N^2$ variables because of the covariance matrices while the proposed observer only requires N variables. Furthermore, the gain of nonlinear Kalman filters is varying and evaluated on-line, which may be computationally demanding, while the gain of the proposed observer is constant and determined off-line. □

D. Corrected estimated concentrations

The observers in Sections V-B and V-C generate estimated lithium concentrations, which can be corrected along with $\hat{c}_{\text{neg},1}$ so that they asymptotically match the concentrations of the PDEs in (1)-(2) for constant input currents as seen in Section III. We note that from $\hat{x}$, which represents the concatenation of the estimated concentrations generated by the chosen observer $\hat{x} = (\hat{c}_{\text{neg},2},\dots,\hat{c}_{\text{neg},N_{\text{neg}}},\hat{c}_{\text{pos},1},\dots,\hat{c}_{\text{pos},N_{\text{pos}}})$, we can retrieve $\hat{c}_{\text{neg},1}$ by replacing the concentrations in (25) by their estimates. We denote in the following $c_{s,(1)}$ the concentrations generated by the PDE model in (1)-(2) as in Section III and $\hat{c}_s$ the estimated concentrations of electrode s, with $s \in \{\text{pos},\text{neg}\}$, given by (33) where L is obtained either from Assumption 2 or by verifying the conditions of Theorem 3.

We denote the corrected estimated concentrations as $\hat{c}_{s,\text{cor}}$, which are given by, for $j \in \{1,\dots,N_s\}$ and $s \in \{\text{neg},\text{pos}\}$,

$$\hat{c}_{\text{s,cor,j}} := \hat{c}_{s,\text{mean}} - K^s_j(\hat{c}_{s,\text{mean}} - \hat{c}_{s,j}), \tag{47}$$

where $\hat{c}_{s,\text{mean}} := \frac{1}{V_s}\sum_{i=1}^{N_s} V^s_i \hat{c}_{s,i}$ and K^s_j defined in (6).

The next theorem states an asymptotic property of the error between the corrected estimated concentrations and the concentrations generated by the original PDEs in (1)-(2) when time tends to infinity in absence of disturbances and noises for constant inputs.

Theorem 4: Consider system (27) and its corresponding observer (33) and suppose $e = x-\hat{x} = 0$ is globally exponentially stable when $w = 0$ and $v = 0$. Then, for any constant input current I_{cell}, any corresponding solution $\hat{x}$ to (33) and $c_{s,(1)}$ to (1)-(2) with $c_{s,(1),\text{mean}}(0)$ equal to the initial mean lithium concentration of electrode s given by x satisfy

$$(\hat{c}_{\text{cor}} - c_{(1)})_\infty = 0, \tag{48}$$

where $\hat{c}_{\text{cor}} := (\hat{c}_{\text{neg,cor},1},\hat{c}_{\text{neg,cor},2},\dots,\hat{c}_{\text{neg,cor},N_{\text{neg}}},\hat{c}_{\text{pos,cor},1},\dots,\hat{c}_{\text{pos,cor},N_{\text{pos}}})$ is the vector of the corrected estimated concentrations and $c_{(1)} := (c_{\text{neg},(1)}(r^{\text{neg}}_1,\cdot),c_{\text{neg},(1)}(r^{\text{neg}}_2,\cdot),\dots,c_{\text{neg},(1)}(r^{\text{neg}}_{N_{\text{neg}}},\cdot),c_{\text{pos},(1)}(r^{\text{pos}}_1,\cdot),\dots,c_{\text{pos},(1)}(r^{\text{pos}}_{N_{\text{pos}}},\cdot))$. □

Proof. We consider system (27), (33) and suppose $e = x-\hat{x} = 0$ is globally exponentially stable when $w = 0$ and $v = 0$. Let I_{cell} be a constant input, $c_{s,(1)}$ be the corresponding solution to (1)-(2) and $(x,\hat{x})$ be a corresponding solution to (27), (33) with $c_{s,(1),\text{mean}}(0)$ equal to the initial mean lithium concentration of electrode s given by x. We thus have $(\hat{x}-x)_\infty = 0$ and $(\hat{c}_{\text{neg},1} - c_{\text{neg},1})_\infty = 0$. Hence, in view of (5) and (47)

$$(\hat{c}_{\text{cor}} - c_{\text{cor}})_\infty = 0, \tag{49}$$

where $c_{\text{cor}} := (c_{\text{neg,cor},1},c_{\text{neg,cor},2},\dots,c_{\text{neg,cor},N_{\text{neg}}},c_{\text{pos,cor},1},\dots,c_{\text{pos,cor},N_{\text{pos}}})$ and $\hat{c}_{\text{cor}} := (\hat{c}_{\text{neg,cor},1},\hat{c}_{\text{neg,cor},2},\dots,\hat{c}_{\text{neg,cor},N_{\text{neg}}},\hat{c}_{\text{pos,cor},1},\dots,\hat{c}_{\text{pos,cor},N_{\text{pos}}})$.

In view of Theorem 1, we have that $(c_{s,\text{cor},j} - c_{s,(1)}(r^s_j,\cdot))_\infty = 0$ for any $j \in \{1,\dots,N_s\}$ and $s \in \{\text{neg},\text{pos}\}$. Therefore, we obtain

$$(c_{\text{cor}} - c_{(1)})_\infty = 0, \tag{50}$$

where $c_{(1)} := (c_{\text{neg},(1)}(r^{\text{neg}}_1,\cdot),c_{\text{neg},(1)}(r^{\text{neg}}_2,\cdot),\dots,c_{\text{neg},(1)}(r^{\text{neg}}_{N_{\text{neg}}},\cdot)$ $,c_{\text{pos},(1)}(r^{\text{pos}}_1,\cdot),\dots,c_{\text{pos},(1)}(r^{\text{pos}}_{N_{\text{pos}}},\cdot)$. From (49) and (50), we derive $(\hat{c}_{\text{cor}} - c_{(1)})_\infty = 0$ as in (48), which completes the proof. ■

Theorem 4 implies that, under the conditions of Theorems 2 or 3, the estimated corrected lithium concentrations asymptotically match the lithium concentrations of the PDEs in (1)-(2) in absence of noise and disturbance provided that a constant input current is applied.

VI. Numerical case study

In this section, we illustrate numerically the benefits of the new, corrected model and the associated state estimation scheme. For this purpose, we consider the infinite-dimensional model in [29] as a reference model and we first compare it with the model in [7] without correction and model (27) with correction considering a uniform volume discretization method (i.e, $V_i^s = \frac{V_s}{N_s}$ for $i \in \{1,\dots,N_s\}$) as done in [7] (Section VI-A). Next, we synthesize observers based on the polytopic approach for the model in [7] and model (27) using Theorem 3 (the conditions of Theorem 2 were not satisfied) and then we compare the obtained estimated variables (Section VI-B).

We simulate model (27) and the model in [7] with the parameters values given in Table I corresponding to a lithium-ion battery cell with a graphite negative electrode and a nickel cobalt aluminium (NCA) positive electrode. We assume that the particles in each electrode are discretized into 4 samples of uniform volume. Consequently, $N_{\text{neg}} = N_{\text{pos}} = 4$ and $N = 4+4-1 = 7$; recall that the concentration at the center of the negative is electrode can be removed as explained in Section IV-B. No measurements noise or perturbations are considered when simulating the two models. The OCVs curves of the battery cell are given in Figure 3. These OCVs are extrapolated using first order approximations on $(-\infty, 0]$ and $[1, \infty)$, respectively, which implies that the OCVs are globally Lipschitz on $\mathbb{R}$ and thus satisfy Assumption 1 as explained in Section V-A. In particular, Assumption 1 holds with $C_{\text{neg},1} = -75.2267$ V, $C_{\text{neg},2} = -0.0067$ V, $C_{\text{pos},1} = -1266.7$ V, $C_{\text{pos},2} = -0.2667$ V. The used input current u is a Plug-in Hybrid Electrical Vehicle (PHEV) discharge current on the time interval $[0, 1800]$, a PHEV charge current on the time interval $[1800, 3600]$ and 0 A on $[3600, 4500]$, as illustrated in Figure 4. It is derived from a PHEV power profile given in [30]. The current profile is thus rapidly varying on [0,3600], during which we will see that improvements are obtained with the corrections presented in Section III. We initialize both models at equilibrium, meaning that all the initial concentrations within the same electrode are equal, with a SOC equal to 100%. The SOC is defined by for $s \in \{\text{pos, neg}\}$

$$SOC_s := 100 \frac{c_{s,\text{mean}} - c_0^s}{c_{100}^s - c_0^s}, \tag{51}$$

where c_0^s, c_{100}^s are the lithium concentration of electrode s at SOC equal 0% and 100%, respectively, see Table I. We note that $c_{s,\text{mean}} := \frac{1}{N_s} \sum_{i=1}^{N_s} c_{s,i}$ (recall that the discretization method we chose is a uniform volume discretization). Given that SOC_{pos} and SOC_{neg} are equal, we use the notation SOC instead. As for the reference model, it is obtained by solving the PDEs of (1) with (2) as boundary conditions using a finite elements method and simulated with the parameters of Table I, see [29] for details.

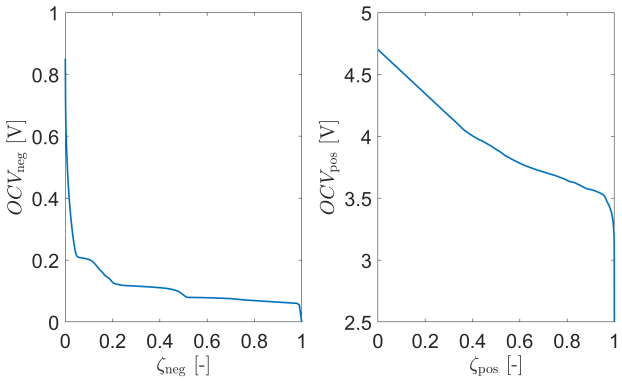

Figure 3. OCVs curves.

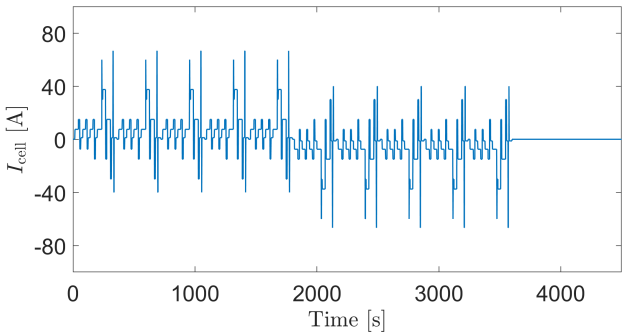

Figure 4. Input current profile.

A. Models comparison

We have compared the output voltages V_{cell} and the surface concentrations $c_{s,\text{surf}}$ generated by the model in [7] and model (27), with those generated by the reference infinite-dimensional model in Figures 5 and 6, respectively, over the whole interval of time [0,4500] as well as [0,3600] where the current is rapidly varying. We see that, in all cases, the proposed corrections allow improving the accuracy of the data even over short time horizons and when the input is rapidly changing. We note that the considered surface concentrations of the reference infinite-dimensional model are those taken at the electrodes/separator interfaces. To quantify this improvement, we have computed the mean absolute error (MAE) and the root mean square error (RMSE) of the voltage error $e_{V_{\text{cell}}}$ between V_{cell} generated by model (1)-(2) and V_{cell} generated by the model in [7] and model (27), respectively. We similarly computed the normalized surface concentrations error $\mathbf{e}_{c_{s,\text{surf}}}$ between the surface concentrations generated by model (1)-(2) and those generated by the model in [7] and model (27), respectively. The results are given in Table II. Model (27) is more accurate than the one in [7]. In particular, we see improvements of the order of 50% for the output voltage, 50% for the surface concentration of the positive electrode and 30% for the surface concentration of the negative electrode on the interval [0,4500] and particularly on [0,3600], when the current is rapidly varying.

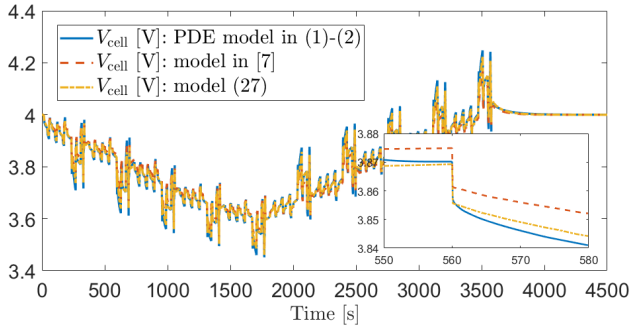

Figure 5. Output voltage.

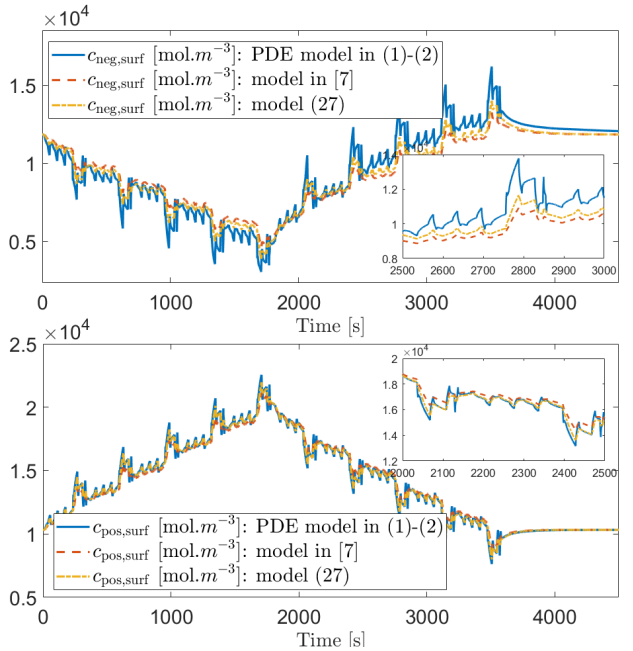

Figure 6. Surface concentrations.

B. State estimation

We have designed observer (33) for system (27) by applying[1] Theorem 3, as (46) holds for the considered parameter values taking $L = 10^4(3.2387, 3.5432, 3.3896, -5.0388, -5.7421, -5.3310, -5.433750)$, $P =$

$$10^{-9}\begin{pmatrix} 0.0137 & 0.0258 & 0.0329 & 0.0066 & 0.0107 & 0.0135 & 0.0149 \\ 0.0258 & 0.0550 & 0.0797 & 0.0127 & 0.0220 & 0.0304 & 0.0361 \\ 0.0329 & 0.0797 & 0.1485 & 0.0179 & 0.0312 & 0.0474 & 0.0681 \\ 0.0066 & 0.0127 & 0.0179 & 0.0136 & 0.0095 & 0.0039 & -0.0031 \\ 0.0107 & 0.0220 & 0.0312 & 0.0095 & 0.0117 & 0.0115 & 0.0077 \\ 0.0135 & 0.0304 & 0.0474 & 0.0039 & 0.0115 & 0.0190 & 0.0231 \\ 0.0149 & 0.0361 & 0.0681 & -0.0031 & 0.0077 & 0.0231 & 0.0471 \end{pmatrix},$$

$\varepsilon = 1.17^*10^{-22}$, $\mu_v = 7.9784$ and $\mu_w = 1.0486$. For the sake of comparison, we have designed an observer for the non-corrected model (30) using the technique in [6], which ensures Assumption 2 holds with the same gain L. The only difference between the two observers is the output equation used to synthesize them. We have initialized both observers such that all estimated concentrations within the same particle are equal and correspond to a SOC estimate, denoted $\widehat{SOC}$, of 0%. We note that $\widehat{SOC}$ is obtained by replacing $c_{s,\text{mean}}$ in (51) by its estimate $\hat{c}_{s,\text{mean}}$. In practical applications, we only know a biased version of the input current u and the output voltage y. This bias is due to the precision of the sensors and their conditioning. Therefore, to account for this bias on the input current and on the output voltage, we take $w(t) = 3\sin(2000\pi t)$, $E = B$, $v(t) = 0.05\sin(200\pi t)$ and $D = 1$.

[1]We have not been able to ensure condition (37) using the observer design technique in [6]. Nevertheless, this is not an issue, as, again, an observer for the corrected model can be synthesized using Theorem 3.

Table II
MAE AND RMSE OF THE OUTPUT VOLTAGE AND THE SURFACE CONCENTRATIONS ERRORS GIVEN BY THE MODEL IN [7] AND MODEL (27)

	MAE [0,4500]	RMSE [0,4500]	MAE [0,3600]	RMSE [0,3600]
$e_{V_{\text{cell}}}$: model in [7] [mV]	12.07	17.76	14.57	19.80
$e_{V_{\text{cell}}}$: model (27) [mV]	**5.07**	**8.28**	**6.09**	**9.23**
Improvement [%]	**58.0**	**53.4**	**58.2**	**53.4**
$\mathbf{e}_{c_{\text{pos,surf}}}$: model in [7] [%]	2.05	3.01	2.48	3.36
$\mathbf{e}_{c_{\text{pos,surf}}}$: model (27) [%]	**0.95**	**1.53**	**1.15**	**1.71**
Improvement [%]	**53.7**	**49.2**	**53.6**	**49.1**
$\mathbf{e}_{c_{\text{neg,surf}}}$: model in [7] [%]	8.51	11.79	9.93	13.10
$\mathbf{e}_{c_{\text{neg,surf}}}$: model (27) [%]	**5.48**	**7.79**	**6.24**	**8.62**
Improvement [%]	**35.6**	**33.9**	**37.2**	**34.2**

Figure 7 reports the actual SOC given by the infinite-dimensional model and the estimated ones, as well as the corresponding norm of the estimation errors on the SOC $e_{SOC} = SOC - \widehat{SOC}$ obtained with the observer in [6], observer (33) and observer (33) with the correction of its estimated concentrations $\hat{c} := (\hat{c}_{\text{neg},1}, \hat{x})$ as done in Theorem 4. We see that observer (33) based on the corrected model (27) provides a more accurate SOC. This improvement is quantified by computing the average MAE and the average RMSE of the SOC estimation errors e_{SOC} for the observer in [6], observer (33) and observer (33) with $\hat{c}_{\text{cor}}$, respectively, averaged over 21 simulations for initial SOC estimates ranging from $\{0\%, 5\%, \ldots, 100\%\}$ and for different gains values L, $10L$ and $L/10$. The results are given in Table III, where the percentages in parenthesis represent the improvement of the associated observer compared to the observer in [6]. We see that observer (33) generates more accurate results in terms of SOC estimation and this improvement is of the order of the percent, which is significant for lithium-ion batteries.

We have also computed in Table III the average MAE and the average RMSE, over the same 21 scenarios and for the same 3 gains, of the normalized estimated concentrations error $\mathbf{e}_{c_s}$ for $s \in \{\text{pos}, \text{neg}\}$, for the observer in [6], for observer (33) and for observer (33) followed by the correction of the estimated concentrations ($\hat{c}_{\text{cor}}$). The normalized estimated concentrations error $\mathbf{e}_{c_s}$ is defined as follows

$$\mathbf{e}_{c_s} := \frac{|c_s - \hat{c}_s|}{|c_s|}, \tag{52}$$

where $c_s := (c_s(r_1^s, \cdot), c_s(r_2^s, \cdot), c_s(r_3^s, \cdot), c_s(r_4^s, \cdot))$ is the vector of concentrations generated by (1)-(2) at the electrodes/separator interfaces and $\hat{c}_s$ is the vector of estimated concentrations generated by the chosen observer. Table III reports that more accurate estimated concentrations are obtained as a result of the correction of the estimated concentrations.

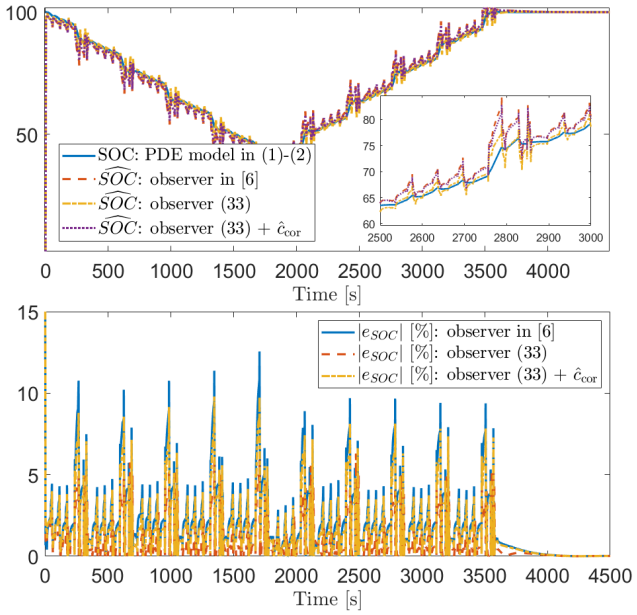

Figure 7. SOC and $\widehat{SOC}$ generated by the observer in [6], observer (33) and observer (33) with $\hat{c}_{\text{cor}}$ (top) and norm of the estimation errors $e_{SOC} := SOC - \widehat{SOC}$ (bottom).

In the following, we go beyond the numerical results presented in this section by feeding the observers implemented on MATLAB with an experimentally measured input current and output voltage.

Remark 5: The improvements observed in this section thanks to the proposed model correction and associated observer become even more significant when considering constant currents, as met in practice in most battery charging processes and consistently with Theorem 1. For instance, we have considered the observer in [6] and observer (33) of Section VI-B with the same gain L. We fed them by a constant current charging profile that is equal to -36 A (charging C-rate : 6C) on the interval $[0,500]$ and 0 A on $[500,1500]$ and by the output voltage generated by an infinite-dimensional model. Then, we compared the observers by computing the average MAE and RMSE on the SOC estimation for initial SOC estimates ranging from $\{0\%,5\%,\ldots,100\%\}$. We have obtained that observer (33) based on the corrected model generates about 80% more accurate SOC estimates than the observer in [6] based on the model without correction. □

VII. Experimental validation

In this section, an experimental validation of the obtained results is carried out on a 6 Ah lithium-ion battery cell, fitted with a graphite negative electrode and a NCA positive electrode. The cell parameters required for model computation are detailed in Table I. We note that some of these parameters are taken from [31] (electrode thicknesses, particle radius, volume fractions, electronic and ionic conductivities), the others have been estimated by experimental characterizations. The OCV curves for the battery cell are as in Figure 3. The cell current and voltage are measured using sensors. We thus obtain the current input shown in Figure 8, which represents

Table III
Average MAE and RMSE over 21 simulations of the SOC estimation errors and of the estimated concentrations errors for different gain values. The values in parenthesis represent the percentage of improvement with respect to the observer in [6]

		MAE	RMSE
L	e_{SOC}: observer in [6] [%]	1.92	2.76
	e_{SOC}: observer (33) [%]	**0.81 (57.8)**	**1.35 (51.1)**
	e_{SOC}: observer (33) + $\hat{c}_{\text{cor}}$ [%]	1.58	2.29
	$\mathbf{e}_{c_{\text{pos}}}$: observer in [6] [%]	1.16	1.87
	$\mathbf{e}_{c_{\text{pos}}}$: observer (33) [%]	1.79	2.35
	$\mathbf{e}_{c_{\text{pos}}}$: observer (33) + $\hat{c}_{\text{cor}}$ [%]	**1.02 (12.1)**	**1.65 (11.8)**
	$\mathbf{e}_{c_{\text{neg}}}$: observer in [6] [%]	5.82	6.5
	$\mathbf{e}_{c_{\text{neg}}}$: observer (33) [%]	7.28	8.18
	$\mathbf{e}_{c_{\text{neg}}}$: observer (33) + $\hat{c}_{\text{cor}}$ [%]	**4.99 (14.3)**	**5.57 (14.3)**
$10L$	e_{SOC}: observer in [6] [%]	1.95	2.81
	e_{SOC}: observer (33) [%]	**0.88 (54.9)**	**1.43 (49.1)**
	e_{SOC}: observer (33) + $\hat{c}_{\text{cor}}$ [%]	1.61	2.33
	$\mathbf{e}_{c_{\text{pos}}}$: observer in [6] [%]	1.26	1.90
	$\mathbf{e}_{c_{\text{pos}}}$: observer (33) [%]	1.89	2.40
	$\mathbf{e}_{c_{\text{pos}}}$: observer (33) + $\hat{c}_{\text{cor}}$ [%]	**1.13 (10.3)**	**1.66 (12.6)**
	$\mathbf{e}_{c_{\text{neg}}}$: observer in [6] [%]	5.81	6.49
	$\mathbf{e}_{c_{\text{neg}}}$: observer (33) [%]	7.28	8.15
	$\mathbf{e}_{c_{\text{neg}}}$: observer (33) + $\hat{c}_{\text{cor}}$ [%]	**4.97 (14.5)**	**5.57 (14.2)**
$L/10$	e_{SOC}: observer in [6] [%]	1.9	2.89
	e_{SOC}: observer (33) [%]	**0.73 (61.6)**	**1.63 (43.6)**
	e_{SOC}: observer (33) + $\hat{c}_{\text{cor}}$ [%]	1.59	2.53
	$\mathbf{e}_{c_{\text{pos}}}$: observer in [6] [%]	1.12	2.42
	$\mathbf{e}_{c_{\text{pos}}}$: observer (33) [%]	1.82	2.86
	$\mathbf{e}_{c_{\text{pos}}}$: observer (33) + $\hat{c}_{\text{cor}}$ [%]	**1.05 (6.25)**	**2.34 (3.3)**
	$\mathbf{e}_{c_{\text{neg}}}$: observer in [6] [%]	5.82	6.54
	$\mathbf{e}_{c_{\text{neg}}}$: observer (33) [%]	7.31	8.22
	$\mathbf{e}_{c_{\text{neg}}}$: observer (33) + $\hat{c}_{\text{cor}}$ [%]	**5.02 (13.7)**	**5.65 (13.6)**

a PHEV discharge current on the interval [0,3240] and 0 A on [3240,3844], and the measured output voltage shown in Figure 9.

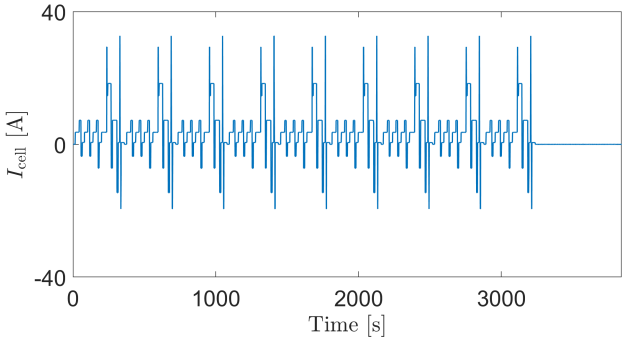

Figure 8. Measured input current.

We first compare the output voltages of both model [7] without correction and model (27) with correction considering a uniform volume discretization as in [7]. For this purpose, we feed both models with a corrected version of the measured current of Figure 8. This current correction is done via a multiplicative gain equal to 1.035, which is chosen such that the measured output voltage and the output voltage obtained by the infinite-dimensional model in [29] match in the terminal steady state. We have calculated the MAE and RMSE of the voltage error $e_{V_{\text{cell}}}$ between the measured output voltage and the voltage generated by the model in [7] and model (27),

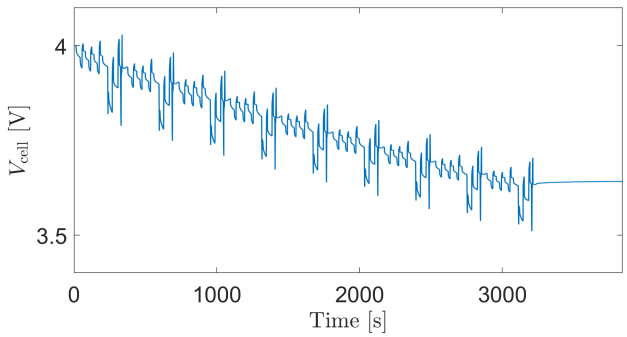

Figure 9. Measured output voltage.

respectively. We have obtained the results of Table IV. We see that the output voltage of the corrected model is about 25% more accurate than the model in [7].

Table IV
MAE AND RMSE OF THE OUTPUT VOLTAGE GIVEN BY THE MODEL IN [7] AND MODEL (27)

	MAE [0,3844]	RMSE [0,3844]	MAE [0,3240]	RMSE [0,3240]
$e_{V_{\text{cell}}}$: model in [7] [mV]	9.35	13.92	11.02	15.16
$e_{V_{\text{cell}}}$: model (27) [mV]	**7.00**	**10.31**	**8.21**	**11.23**
Improvement [%]	**25.1**	**25.9**	**25.5**	**25.92**

Next, we consider the observers designed in Section VI-B of gain L with the same initialization. However, in this section, we feed them with the measured input current and output voltage obtained by experimentation. To compare the output voltage and SOC estimated by both observers, we take as a reference the measured output voltage and the experimental SOC calculated by integration of the corrected measured current as follows

$$SOC_{\text{exp}}(t) := -\frac{1}{3600 Q_{\text{cell}}} \int_0^t I_{\text{cell, cor}}(\tau) d\tau, \qquad (53)$$

where $I_{\text{cell, cor}}$ is the corrected measured input current.

Figure 10 shows the experimental SOC and the estimated ones, as well as the corresponding norm of the estimation error $e_{SOC} := SOC_{\text{exp}} - \widehat{SOC}$. Observer (33) generates the most accurate SOC estimates. We quantified the results by computing the average MAE and the average RMSE of the estimation errors for each of the observer in [6], observer (33) and observer (33) with $\hat{c}_{\text{cor}}$ over the same 21 scenarios. The results are shown in Table V. The values in parenthesis represent the improvement of the corresponding observer with respect to the observer in [6]. Observer (33) has the least SOC estimation error. In particular, observer (33) based on the corrected model estimates the state of charge about 25% more accurately than the observer in [6].

In addition, we also computed the MAE and RMSE of the voltage error between the measured output voltage and the estimated output voltages generated by the observer in [6] and observer (33) averaged over the same 21 scenarios. The results are also shown in Table V. The voltage error associated to observer (33) is lower than that of the model in [6]. Hence, observer (33) also estimates the output voltage more precisely than the observer in [6].

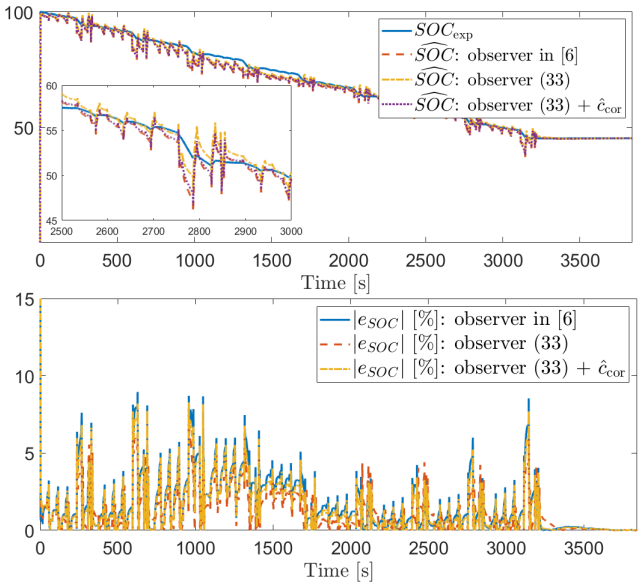

Figure 10. SOC_{exp} and $\widehat{SOC}$ generated by the observer in [6], observer (33) and observer (33) with $\hat{c}_{\text{cor}}$ (top) and norm of the estimation errors $e_{SOC} := SOC_{\text{exp}} - \widehat{SOC}$ (bottom).

Table V
AVERAGE MAE AND RMSE OVER 21 SCENARIOS OF THE SOC ESTIMATION ERRORS AND OF THE ESTIMATED VOLTAGE ERRORS. THE VALUES IN PARENTHESIS REPRESENT THE PERCENTAGE OF IMPROVEMENT WITH RESPECT TO THE OBSERVER IN [6]

	MAE	RMSE
e_{SOC}: observer in [6] [%]	1.57	2.33
e_{SOC}: observer (33) [%]	**1.16 (26.1)**	**1.75 (24.9)**
e_{SOC}: observer (33) + $\hat{c}_{\text{cor}}$ [%]	1.40	2.11
$e_{V_{\text{cell}}}$: observer in [6] [mV]	0.53	3.27
$e_{V_{\text{cell}}}$: observer (33) [mV]	**0.50 (5.7)**	**3.23 (1.2)**

VIII. CONCLUSION

We have presented an approach to correct the lithium concentrations of a finite-dimensional SPM to asymptotically eliminate the errors induced by the PDE discretization for constant currents. As a result, more accurate variables are generated by the finite-dimensional model as illustrated in simulations. We have then exploited these corrections to derive a new output voltage equation and thus a new state space model. Two observer design strategies have been proposed for this new model, with robust stability guarantees. The estimated variables generated by the chosen observer are then corrected to also asymptotically match those of the PDEs. The obtained simulation and experimentation results show significant improvement in terms of state estimation. Among the possible future works we can envision is the design of sampled-data observers for real-time implementation.

APPENDIX A
PROOF OF (8)

The mean concentration $c_{s,(1),\text{mean}}$ is given in (3). We have for all $t \geq 0$,

$$c_{s,(1),\text{mean}}(t) = \frac{1}{V_s}\int_0^{R_s} 4\pi r^2 c_s(r,t)dr = \frac{3}{R_s^3}\int_0^{R_s} r^2 c_s(r,t)dr. \tag{54}$$

In view of (1), we have for all $t \geq 0$ and $r \in [0,R_s]$

$$r^2\frac{\partial c_s(r,t)}{\partial t} = \frac{\partial}{\partial r}\left(D_s r^2 \frac{\partial c_s(r,t)}{\partial r}\right) = \frac{\partial}{\partial r}\left(-r^2\varphi_s(r,t)\right). \tag{55}$$

By integrating (55) on $[0,R_s]$, we obtain

$$\int_0^{R_s} r^2\frac{\partial c_s(r,t)}{\partial t}dr = -R_s^2\varphi_s(R_s,t). \tag{56}$$

From (54) and (56), we get

$$\int_0^{R_s} r^2\frac{\partial c_s(r,t)}{\partial t}dr = \frac{d}{dt}\left(\frac{R_s^3}{3}c_{s,(1),\text{mean}}(t)\right) = -R_s^2\varphi_s(R_s,t). \tag{57}$$

From (57), in view of the boundary conditions in (2), $\dot{c}_{s,(1),\text{mean}} = -\frac{3}{R_s}\frac{j_s^{\text{Li}}(t)}{a_s F}$. By the definition of a_s, we thus derive (8).

APPENDIX B
PROOF OF PROPOSITION 1

Solutions to (1)-(2) for any given Lebesgue measurable, locally essentially bounded input m_s, can be obtained using a solution decomposition technique as follows.

We first drop the notation $c_{s,(1)}$ to refer to the lithium concentrations generated by the PDEs in (1)-(2). Let m_s be a Lebesgue measurable, locally essentially bounded input, $c_{s,1}$ be a solution to (1)-(2) with input m_s and $c_{s,1}(r,0) = c_0(r)$, $c_{s,2}$ be a solution to (1)-(2) with input m_s and $c_{s,2}(r,0) = \bar{c}_0$ for any $r \in [0,R_s]$, $\bar{c}_0 \in \mathbb{R}_{\geq 0}$ being the initial mean concentration $c_{s,1,\text{mean}}(0)$ and $c_{s,3}$ a solution to (1) with input m_s, $c_{s,3}(r,0) = c_0(r) - \bar{c}_0$ and the boundary conditions being $\varphi_s(0,t) = 0$ and $\varphi_s(R_s,t) = 0$. We have $c_{s,1}(r,t) = c_{s,2}(r,t) + c_{s,3}(r,t)$ for all $t \geq 0$ and $r \in [0,R_s]$ by linearity of (1). Let $y(r,t) = rc_{s,3}(r,t)$, from (1), we derive for all $t \geq 0$ and $r \in [0,R_s]$

$$\frac{\partial y(r,t)}{\partial t} = D_s\frac{\partial^2 y(r,t)}{\partial r^2}. \tag{58}$$

The solution to (58) is derived using the variable separation method and $c_{s,3}$ boundary conditions. We thus obtain for all $t \geq 0$ and all $r \in [0,R_s]$

$$c_{s,3}(r,t) = \sum_{n=1}^{\infty} B_n\frac{\sin(\lambda_n r)}{r}e^{-\lambda_n^2 D_s t}, \tag{59}$$

where λ_n is the series of strictly positive solutions to $\lambda R_s = \tan(\lambda R_s)$ and the coefficients B_n satisfy

$$B_n = \frac{2}{R_s}\frac{\int_0^{R_s} rc_0(r)\sin(\lambda_n R_s)dr}{\sin^2(\lambda_n R_s)}. \tag{60}$$

In view of (59), we derive for any $r \in [0,R_s]$

$$(c_{s,3}(r,\cdot))_\infty = 0. \tag{61}$$

From (61) and as $c_{s,1}(r,t) = c_{s,2}(r,t) + c_{s,3}(r,t)$, we deduce the desired result, namely (9), holds.

APPENDIX C
PROOF OF LEMMA 3

We first show that all the eigenvalues of matrix A_s are non-positive (note that these are real as A_s is a tridiagonal matrix with symmetric coefficients signs). We invoke for this purpose Gersgorin disk theorem. This theorem states that each eigenvalue λ_m, with $m \in \{1,\ldots,N_s\}$, of A_s satisfies at least one the inequalities $|\lambda_m - (A_s)_{ii}| \leq \rho_i$ with $\rho_i := \sum_{\substack{j=1 \\ j\neq i}}^{N_s} |(A_s)_{ij}|$ for $i \in \{1,\ldots,N_s\}$. In view of the expression of A_s, this means that each λ_m of A_s satisfies at least one of the inequalities $|\lambda_m + \mu_1^s| \leq \mu_1^s$, $|\lambda_m + \upsilon_i^s| \leq \upsilon_i^s$ for $i \in \{2,\ldots,N_s-1\}$ and $|\lambda_m + \tilde{\mu}_{N_s}^s| \leq \tilde{\mu}_{N_s}^s$. Hence, we deduce that $\lambda_m \leq 0$ for all $m \in \{1,\ldots,N_s\}$. On the other hand, by solving $A_s x = \mathbf{0}_{N_s\times 1}$ for any $x \in \mathbb{R}^{N_s}$, we derive $\ker(A_s) = \{\alpha\mathbf{1}_{N_s\times 1} : \alpha \in \mathbb{R}\}$ is of dimension 1. Hence, the rank of A_s is $N_s - 1$, which means that there is a single eigenvalue of A_s that is equal to 0. Consequently, A_s admits $N_s - 1$ strictly negative eigenvalues.

Let $\lambda_m \in \mathbb{R}_{<0}$ be an eigenvalue of A_s, let x_m be a corresponding non-zero eigenvector, i.e., $A_s x_m = \lambda_m x_m$ and $x_m \neq 0$. Given that $\Gamma_s A_s = \mathbf{0}_{1\times N_s}$, we derive $\Gamma_s A_s x_m = \Gamma_s\lambda_m x_m = \mathbf{0}_{1\times N_s}$. Thus, as $\lambda_m \neq 0$, we obtain

$$\sum_{i=1}^{N_s} V_i^s x_{m,i} = 0. \tag{62}$$

On the other hand, $A_s x_m = \lambda_m x_m$ is equivalent to, for any $i \in \{1,\ldots,N_s\}$

$$\sum_{j=1}^{N_s}(A_s)_{ij}x_{m,j} = \lambda_m x_{m,i}. \tag{63}$$

Using (62), we obtain $x_{m,N_s} = -\frac{1}{V_{N_s}^s}\sum_{i=1}^{N_s-1} V_i^s x_{m,i}$. Hence, (63) is equivalent to $\sum_{j=1}^{N_s-1}(A_s)_{ij}x_{m,j} + (A_s)_{iN_s}x_{m,N_s} = \sum_{j=1}^{N_s-1}(A_s)_{ij}x_{m,j} - \frac{1}{V_{N_s}^s}\sum_{j=1}^{N_s-1}(A_s)_{iN_s}V_j^s x_{m,j} = \lambda_m x_{m,i}$. Therefore, in view of the definition of $\tilde{A}_s$ we derive for any $i \in \{1,\ldots,N_s-1\}$

$$\sum_{j=1}^{N_s-1}\left((A_s)_{ij} - (A_s)_{iN_s}\frac{V_j^s}{V_{N_s}^s}\right)x_{m,j} = \sum_{j=1}^{N_s-1}(\tilde{A}_s)_{ij}x_{m,j} = \lambda_m x_{m,i}. \tag{64}$$

From (64), we obtain $\tilde{A}_s\tilde{x}_m = \lambda_m\tilde{x}_m$, where $\tilde{x}_m$ is the vector of the $N_s - 1$ first coefficients of x_m. Therefore, λ_m is an eigenvalue of $\tilde{A}_s$. Consequently, any of the $N_s - 1$ strictly negative eigenvalue of A_s is also an eigenvalue of $\tilde{A}_s$. Since $\tilde{A}_s$ is of dimension $N_s - 1 \times N_s - 1$, this implies that all the eigenvalues of $\tilde{A}_s$ are strictly negative: matrix $\tilde{A}_s$ is Hurwitz. Lemma 3 is thus proven.

REFERENCES

[1] M. A. Hannan, M. S. H. Lipu, A. Hussain, and A. Mohamed, "A review of lithium-ion battery state of charge estimation and management system in electric vehicle applications: Challenges and recommendations," *Renewable and Sustainable Energy Reviews*, vol. 78, pp. 834–854, 2017.

[2] J. K. Barillas, J. Li, C. Guenther, and M. A. Danzer, "A comparative study and validation of state estimation algorithms for Li-ion batteries in battery management systems," *Applied Energy*, vol. 155, pp. 455–462, 2015.

[3] E. Chemali, P. J. Kollmeyer, M. Preindl, and A. Emadi, "State-of-charge estimation of Li-ion batteries using deep neural networks: A machine learning approach," *Journal of Power Sources*, vol. 400, pp. 242–255, 2018.

[4] K. S. Ng, C. Moo, Y. Chen, and Y. Hsieh, "Enhanced coulomb counting method for estimating state-of-charge and state-of-health of lithium-ion batteries," *Applied Energy*, vol. 86, no. 9, pp. 1506–1511, 2009.

[5] R. Klein, N. A. Chaturvedi, J. Christensen, J. Ahmed, R. Findeisen, and A. Kojic, "Electrochemical model based observer design for a lithium-ion battery," *IEEE Transactions on Control Systems Technology*, vol. 21, no. 2, pp. 289–301, 2013.

[6] P. Blondel and R. Postoyan and S. Raël and S. Benjamin and P. Desprez, "Observer design for an electrochemical model of lithium-ion batteries based on a polytopic approach," in *IFAC World Congress*, Toulouse, France, 2017, pp. 8127–8132.

[7] P. Blondel, R. Postoyan, S. Raël, S. Benjamin, and P. Desprez, "Nonlinear circle-criterion observer design for an electrochemical battery model," *IEEE Transactions on Control Systems and Technology*, vol. 27, pp. 889–897, 2019.

[8] A. Allam and S. Onori, "An interconnected observer for concurrent estimation of bulk and surface concentration in the cathode and anode of a lithium-ion battery," *IEEE Transactions on Industrial Electronics*, vol. 65, no. 9, pp. 7311–7321, 2018.

[9] A. Allam and S. Onori, "Online capacity estimation for lithium-ion battery cells via an electrochemical model-based adaptive interconnected observer," *IEEE Transactions on Control Systems Technology*, vol. 29, no. 4, pp. 1636–1651, 2021.

[10] S. Dey, B. Ayalew, and P. Pisu, "Nonlinear robust observers for state-of-charge estimation of lithium-ion cells based on a reduced electrochemical model," *IEEE Transactions on Control Systems Technology*, vol. 23, no. 5, pp. 1935–1942, 2015.

[11] H. J. Dreef, H. P. G. J. Beelen, and M. C. F. Donkers, "LMI-based robust observer design for battery state-of-charge estimation," in *IEEE Conference on Decision and Control*, Miami Beach, USA, 2018, pp. 5716–5721.

[12] B. Wang, Z. Liu, S. E. Li, S. Moura, and H. Peng, "State-of-charge estimation for lithium-ion batteries based on a nonlinear fractional model," *IEEE Transactions on Control Systems Technology*, vol. 25, no. 1, pp. 3–11, 2017.

[13] H. He, R. Xiong, H. Guo, and S. Li, "Comparison study on the battery models used for the energy management of batteries in electric vehicles," *Energy Conversion and Management*, vol. 64, pp. 113–121, 2012.

[14] J. Meng, G. Luo, M. Ricco, M. Swierczynski, D.-I. Stroe, and R. Teodorescu, "Overview of lithium-ion battery modeling methods for state-of-charge estimation in electrical vehicles," *Applied Sciences*, vol. 8, no. 5, p. 659, 2018.

[15] Y. Wang, J. Tian, Z. Sun, L. Wang, R. Xu, M. Li, and Z. Chen, "A comprehensive review of battery modeling and state estimation approaches for advanced battery management systems," *Renewable and Sustainable Energy Reviews*, vol. 131, p. 110015, 2020.

[16] M. Doyle, T. F. Fuller, and J. Newman, "Modeling of galvanostatic charge and discharge of the lithium/polymer/insertion cell," *Journal of The Electrochemical Society*, vol. 140, no. 6, p. 1526, 1993.

[17] T. F. Fuller, M. Doyle, and J. Newman, "Simulation and optimization of the dual lithium ion insertion cell," *Journal of The Electrochemical Society*, vol. 141, no. 1, pp. 1–10, 1994.

[18] B. S. Haran, B. N. Popov, and R. E. White, "Determination of the hydrogen diffusion coefficient in metal hydrides by impedance spectroscopy," *Journal of Power Sources*, vol. 75, no. 1, pp. 56–63, 1998.

[19] E. Planté, R. Postoyan, S. Raël, J. Youssef, S. Benjamin, and D. M. Reyes, "Multiple active material lithium-ion batteries: Finite-dimensional modeling and constrained state estimation," *IEEE Transactions on Control Systems Technology*, vol. 31, no. 3, pp. 1106–1121, 2023.

[20] S. Moura, N. A. Chaturvedi, and M. Krstić, "PDE estimation techniques for advanced battery management systems — Part II: SOH identification," in *American Control Conference*, Montréal, Canada, 2012, pp. 559–565.

[21] D. D. Domenico, A. G. Stefanopoulou, and G. Fiengo, "Lithium-ion battery state of charge and critical surface charge estimation using an electrochemical model-based extended Kalman filter," *ASME Journal of Dynamic Systems, Measurement, and Control*, vol. 132, no. 6, pp. 1–11, 2010.

[22] A. Zemouche, M. Boutayeb, and G. Bara, "Observers for a class of Lipschitz systems with extension to H_∞ performance analysis," *Systems & Control Letters*, vol. 57, pp. 18–27, 2008.

[23] M. Khalil, R. Postoyan, and S. Raël, "State estimation for enhanced low dimensional electrochemical models of lithium-ion batteries," in *IEEE Conference on Decision and Control*, Marina Bay Sands, Singapore, 2023, pp. 7514–7519.

[24] G. A. Nazri and O. Pistoia, *Lithium Batteries: Science and Technology*. Kluwer Academic Publishers, 2004.

[25] M. Benzine, R. Postoyan, S. Raël, S. Benjamin, and D. Monier Reyes, "Systematic observer redesign for lithium-ion battery models to account for the electrolyte dynamics," *Submitted for publication*, 2022.

[26] F. Kremer, S. Raël, and M. Urbain, "1D electrochemical model of lithium-ion battery for a sizing methodology of thermal power plant integrated storage system," *AIMS Energy*, vol. 8, no. 5, pp. 721–748, 2020.

[27] Y. Gao, K. Liu, C. Zhu, X. Zhang, and D. Zhang, "Co-estimation of state-of-charge and state-of-health for lithium-ion batteries using an enhanced electrochemical model," *IEEE Transactions on Industrial Electronics*, vol. 69, no. 3, pp. 2684–2696, 2022.

[28] H. K. Khalil, *Nonlinear Systems Third Edition*, ser. Pearson Education. Prentice Hall, 2002.

[29] S. Raël and M. Hinaje, "Using electrical analogy to describe mass and charge transport in lithium-ion batteries," *Journal of Power Sources*, vol. 222, pp. 112–122, 2013.

[30] J. R. Belt, "Battery test manual for plug-in hybrid electric vehicles," *Technical report, Idaho National Laboratory (INL)*, 2010.

[31] K. Smith and C. Wang, "Power and thermal characterization of a lithium-ion battery pack for hybrid-electric vehicles," *Journal of Power Sources*, vol. 160, pp. 662–673, 2006.

Mira Khalil has been a Ph.D. student in Automatic Control at CRAN, GREEN, Université de Lorraine, CNRS, Nancy, France, since 2022. She received the master degree in Electrical and Electronics Engineering and the master degree in Technology of Communication, Medical and, Industrial Systems from the Lebanese University, Lebanon, in 2022. Her research interests include electrochemical batteries, observer design, Lyapunov stability methods and, hybrid systems.

Romain Postoyan received the M.Sc. degree in Electrical and Control Engineering ("Ingénieur en Génie Electrique et Automatique") from ENSEEIHT (France) in 2005. He obtained the M.Sc. by Research in Control Theory and its Applications from Coventry University (United Kingdom) in 2006 and the Ph.D. in Control Engineering from Université Paris-Sud (France) in 2009. In 2010, he was a research assistant at the University of Melbourne (Australia). Since 2011, he is a CNRS researcher at the "Centre de Recherche en Automatique de Nancy" (France). He obtained the "Habilitation à Diriger des Recherches" from Université de Lorraine in 2019. He serves/served as an associate editor for the journals: Automatica, IEEE Control Systems Letters and IMA Journal of Mathematical Control and Information.

Stéphane Raël received the Engineer degree from the École Nationale Supérieure des Ingénieurs Electriciens de Grenoble (ENSIEG), Grenoble, France, in 1992, the Ph.D. degree in electrical engineering from the Institut National Polytechnique de Grenoble (INPG), Grenoble, in 1996, and the "Habilitation à Diriger des Recherches" degree from the Institut National Polytechnique de Lorraine (INPL), Nancy, France, in 2005. In 1998, he became an Assistant Professor at INPL. Since 2008, he has been a Professor with the INPL until 2012, then at the Université de Lorraine, Nancy. His current research interests include power semiconductor devices and electrochemical devices, such as fuel cells, batteries, and supercapacitors.